Revisiting the Complexation of Cm(III) with Aqueous Phosphates: What Can We Learn from the Complex Structures Using Luminescence Spectroscopy and Ab Initio Simulations?

Nina Huittinen, Isabelle Jessat, Florent Réal, Valérie Vallet, Sebastian Starke, Manuel Eibl, Norbert Jordan

Inorganic Chemistry

pubs.acs.org/IC Article

Revisiting the Complexation of Cm(III) with Aqueous Phosphates: What Can We Learn from the Complex Structures Using Luminescence Spectroscopy and *Ab Initio* Simulations?

Nina Huittinen, Isabelle Jessat, Florent Réal,* Valérie Vallet, Sebastian Starke, Manuel Eibl, and Norbert Jordan*

Cite This: *Inorg. Chem.* 2021, 60, 10656−10673 Read Online

ACCESS | Metrics & More | Article Recommendations | Supporting Information

ABSTRACT: The coordination chemistry of Cm(III) with aqueous phosphates was investigated by means of laser-induced luminescence spectroscopy and *ab initio* simulations. For the first time, in addition to the presence of $Cm(H_2PO_4)^{2+}$, the formation of $Cm(H_2PO_4)_2^{+}$ was unambiguously established from the luminescence spectroscopic data collected at various H^+ concentrations ($-\log_{10}$ $[H^+]$ = 2.52, 3.44, and 3.65), ionic strengths (0.5−3.0 mol·L^{-1} $NaClO_4$), and temperatures (25−90 °C). Complexation constants for both species were derived and extrapolated to standard conditions using the specific ion interaction theory. The molal enthalpy $\Delta_R H^0_m$ and molal entropy $\Delta_R S^0_m$ of both complexation reactions were derived using the integrated van't Hoff equation and indicated an endothermic and entropy-driven complexation. For the $Cm(H_2PO_4)_2^{+}$ complex, a more satisfactory description could be obtained when including the molal heat capacity term. While monodentate binding of the $H_2PO_4^-$ ligand(s) to the central curium ion was found to be the most stable configuration for both complexes in our *ab initio* simulations and luminescence lifetime analyses, a different temperature-dependent coordination to hydration water molecules could be deduced from the electronic structure of the Cm(III)−phosphate complexes. More precisely, where the $Cm(H_2PO_4)^{2+}$ complex could be shown to retain an overall coordination number of 9 over the entire investigated temperature range, a coordination change from 9 to 8 was established for the $Cm(H_2PO_4)_2^{+}$ species with increasing temperature.

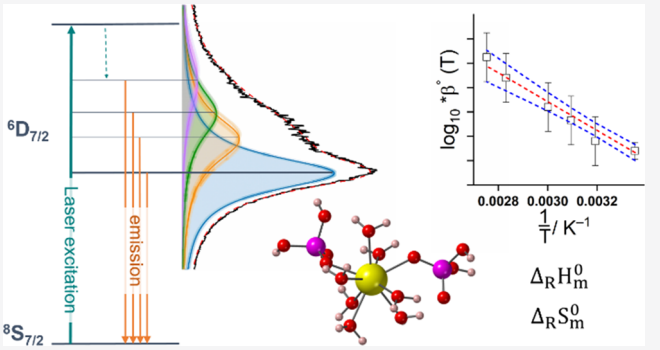

1. INTRODUCTION

The coordination chemistry of actinides (*An*), particularly involving strong inorganic ligands such as carbonate, hydroxide, and phosphate, is an important factor governing their environmental behavior and subsequently their mobility in the (sub)surface.[1−3] Depending on the actinide and inorganic ligand in question, soluble complexes may form in solution, which do not adhere on solid phases due to, *e.g.*, charge constraints, consequently increasing the mobility of the actinide in the surrounding. Alternatively, the solubility of an actinide-bearing solid phase such as hydroxide, oxide, carbonate, or phosphate can be exceeded, leading to precipitation and, potentially, to the immobilization of the actinide. Thus, in order to predict the mobility of radioactive contaminants in natural aquatic systems, especially with regard to the safety of nuclear waste disposal, reliable thermodynamic data such as complexation constants, solubility products, and enthalpies and entropies of reaction are required.

Inorganic phosphates (mainly orthophosphates) in the environment originate from the natural decomposition, or the solubilization mediated by microbial processes, of phosphate-containing rocks and minerals.[4,5] Anthropogenic sources such as fertilizer runoff and the use of phosphate-based detergents locally add to the phosphorus content in the environment.[6−9] In addition, phosphate-containing glasses or crystalline phosphate-based ceramics such as lanthanide (*Ln*) orthophosphates with the monazite structure ($LnPO_4$) may be used for the immobilization of HLW streams for safe storage in deep underground repositories in the future,[10−13] which could locally increase the occurrence of phosphate in the repository. In this context especially trivalent actinides (Cm^{3+}, Am^{3+}) present in, *e.g.*, spent nuclear fuel (SNF) reprocessing waste and plutonium (Pu) originating from the dismantling of

Received: April 30, 2021
Published: June 30, 2021

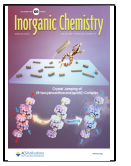

https://doi.org/10.1021/acs.inorgchem.1c01319
Inorg. Chem. 2021, 60, 10656−10673

Table 1. Published Complexation Constants at Infinite Dilution ($\log_{10}\beta°$) for Cm(III)− and Am(III)−Phosphate Complexes

literature	method	complex	$\log_{10}\beta^0$	T (°C)	complex formation reaction
		curium			
Jordan et al.[14]	TRLFS (λ_{exc} = 396.6 nm)[a]	$Cm(H_2PO_4)^{2+}$	2.59 ± 0.19[b]	25	$Cm^{3+} + H_2PO_4^- \rightleftharpoons Cm(H_2PO_4)^{2+}$
			2.73 ± 0.16[b]	40	
			2.83 ± 0.24[b]	50	
			2.96 ± 0.16[b]	60	
			3.11 ± 0.16[b]	80	
Moll et al.[15]	TRLFS (λ_{exc} = 396 nm)[a]	$Cm(H_2PO_4)^{2+}$	2.46 ± 0.13	R.T.[c]	$Cm^{3+} + H_2PO_4^- \rightleftharpoons Cm(H_2PO_4)^{2+}$
		$Cm(HPO_4)^+$	6.21 ± 0.80		$Cm^{3+} + HPO_4^{2-} \rightleftharpoons Cm(HPO_4)^+$
Morgenstern[16]	TRLFS[a]	$Cm(H_2PO_4)^{2+}$	2.71 ± 0.04[d]	R.T.[c]	$Cm^{3+} + H_2PO_4^- \rightleftharpoons Cm(H_2PO_4)^{2+}$
Moskvin[17]	N.A.[e]	$Cm(H_2PO_4)^{2+}$	2.40	N.A.[e]	$Cm^{3+} + H_2PO_4^- \rightleftharpoons Cm(H_2PO_4)^{2+}$
		$Cm(H_2PO_4)_2^+$	3.60		$Cm^{3+} + 2H_2PO_4^- \rightleftharpoons Cm(H_2PO_4)_2^+$
		$Cm(H_2PO_4)_3^0$	5.61		$Cm^{3+} + 3H_2PO_4^- \rightleftharpoons Cm(H_2PO_4)_3^0$
		$Cm(H_2PO_4)_4^-$	6.20		$Cm^{3+} + 4H_2PO_4^- \rightleftharpoons Cm(H_2PO_4)_4^-$
		americium			
Rao et al.[18]	solvent extraction	$Am(H_2PO_4)^{2+}$	2.13 ± 0.08	30	$Am^{3+} + H_2PO_4^- \rightleftharpoons Am(H_2PO_4)^{2+}$
		$Am(HPO_4)^+$	4.14 ± 0.08		$Am^{3+} + HPO_4^{2-} \rightleftharpoons Am(HPO_4)^+$
Borisov et al.[19]	cation exchange	$Am(H_2PO_4)^{2+}$	2.51	20 ± 2	$Am^{3+} + H_2PO_4^- \rightleftharpoons Am(H_2PO_4)^{2+}$
Moskvin[17]	N.A.[e]	$Am(H_2PO_4)^{2+}$	2.39	N.A.[e]	$Am^{3+} + H_2PO_4^- \rightleftharpoons Am(H_2PO_4)^{2+}$
		$Am(H_2PO_4)_2^+$	3.63		$Am^{3+} + 2H_2PO_4^- \rightleftharpoons Am(H_2PO_4)_2^+$
		$Am(H_2PO_4)_3^0$	5.62		$Am^{3+} + 3H_2PO_4^- \rightleftharpoons Am(H_2PO_4)_3^0$
		$Am(H_2PO_4)_4^-$	6.30		$Am^{3+} + 4H_2PO_4^- \rightleftharpoons Am(H_2PO_4)_4^-$
Lebedev et al.[20]	spectrophotometry	$Am(H_2PO_4)^{2+}$	2.73 ± 0.06[f]	23 ± 2	$Am^{3+} + H_2PO_4^- \rightleftharpoons Am(H_2PO_4)^{2+}$
		$Am(H_2PO_4)_2^+$	3.72 ± 0.02[f]		$Am^{3+} + 2H_2PO_4^- \rightleftharpoons Am(H_2PO_4)_2^+$

[a]TRLFS: time-resolved laser-induced fluorescence spectroscopy. [b]Recalculated using the values published by Jordan et al.[14] and the $\log_{10}\beta^0$ and $\Delta_R H_m^0$ values for the reaction $H^+ + H_2PO_4^- \rightleftharpoons H_3PO_4$ at each temperature from Grenthe et al.[21] [c]R.T.: room temperature. [d]From the value recalculated by Moll et al.[15] for the equilibrium $Cm^{3+} + 2H^+ + PO_4^{3-} \rightleftharpoons Cm(H_2PO_4)^{2+}$. [e]N.A.: not available. [f]As mentioned by Silva et al.,[22] the reaction involves exchange between ligands and solvation water molecules and the equilibrium constant was corrected for changes in water activity.

nuclear weapons are potential candidates for such tailored waste matrices.

These actinides are, furthermore, of great importance for the safety case of final waste repositories as Am and especially Pu will dominate the long-term radiotoxicity of spent nuclear fuel (SNF). Under conditions prevailing in deep underground repositories for SNF and high-level waste (HLW) streams, these actinides are found in the trivalent and tetravalent oxidation states, of which the former one is more soluble and, therefore, potentially more mobile.

As already recognized in our previous investigation dealing with the complexation of Eu(III) and Cm(III) with aqueous phosphates at elevated temperatures,[14] studies concerning the complexation reactions of trivalent actinides with various phosphate ligands, *i.e.*, $H_2PO_4^-$, HPO_4^{2-}, or PO_4^{3-}, are rather scarce. One reason for the lack of thermodynamic data for these *An*-orthophosphates is the very low solubility of hydrous $AnPO_4$ solid phases, consequently rendering any experimental determination of the aqueous speciation extremely difficult. In fact, most of the available data exists for the $AnH_2PO_4^{2+}$ complex, prevailing in the acidic pH range with some literature found for $AnHPO_4^+$ (Table 1).

Note that the values of Moskvin[23] determined by ion exchange are not indicated in Table 1 since only conditional constants at I = 1.0 mol·L^{-1} NH_4Cl were reported and not all the required ion interaction coefficients are available for the extrapolation to infinite dilution (Grenthe et al.[21]). Also, note that the values of the stepwise conditional complexation constants reported by Moskvin[17] for Am(III) and Cm(III) do not show the expected decrease with the increase of $H_2PO_4^-$ ligands. For the $Am(H_2PO_4)^{2+}$ complex, Silva et al.[22] (Nuclear Energy Agency (NEA) Thermochemical Database (TDB) Project, vol. 2) recommended a $\log_{10}\beta°$ value at 25 °C, based on the solvent extraction study of Rao et al.[18] Later Morgenstern[16] and Moll et al.[15] reported a $\log_{10}\beta°$ value of very similar magnitude for $Cm(H_2PO_4)^{2+}$, derived from luminescence spectroscopic investigations, which has been recently confirmed.[14] The latest volume of the NEA-TDB[21] recommends a $\log_{10}\beta°$ value for $Cm(H_2PO_4)^{2+}$ based on the study of Moll et al.[15] and assumes this value to be a good approximation for $Am(H_2PO_4)^{2+}$.

No recommended value from the NEA−TDB[21,22] for the complexation constant of the $AnHPO_4^+$ complex exists due to the fact that (i) the stoichiometry of the complex has not been unambiguously proven in the existing literature and (ii) large deviations by more than 2 orders of magnitude between $AmHPO_4^+$ (Rao et al.[18]) and $CmHPO_4^+$ (Moll et al.[15]) were reported. Further complexes such as $An(H_2PO_4)_3^0$ and $An(H_2PO_4)_4^-$ were also reported, but a spectroscopic verification and confirmation of the stoichiometry of the proposed complexes are still missing. In addition, structural data in terms of denticity, bond lengths, and their character, together with the coordination number of the central ion of the accepted actinide phosphate complexes, do, to the best of our knowledge, not exist. Despite the fact that spectroscopic tools have been used for the derivation of thermodynamic data, the changes occurring in the electronic structure of the actinide-complexes under different chemical conditions have not been used to derive such structural data. Thus, this study aims at (i) continuing the stepwise determination of relevant *An*−orthophosphate complexes and their stability constants and thermodynamic data, with a focus on the apparent knowledge gaps in the acidic pH regime and (ii) exploring the coordination chemistry of these species.

https://doi.org/10.1021/acs.inorgchem.1c01319
Inorg. Chem. 2021, 60, 10656−10673

As briefly mentioned, our previous study investigated the complexation of Cm(III) with aqueous phosphates at acidic pH (−log [H^+] = 1.00) using luminescence spectroscopy. At this very acidic pH, only the $H_2PO_4^-$ ligand is present in solution in addition to nondissociated phosphoric acid (H_3PO_4), which facilitated the interpretation of collected spectroscopic data. By conducting the experiments at several ionic strengths (I = 0.6−3.1 mol·L^{-1}), the specific ion interaction theory (SIT) could be used for the extrapolation of the obtained complexation constants to infinite dilution and to extract the first experimentally determined ion interaction coefficient $\varepsilon(Cm(H_2PO_4)^{2+}; ClO_4^-)$. Temperature-dependent investigations in the range of 25−80 °C enabled the extraction of the first thermodynamic function for the $Cm(H_2PO_4)^{2+}$ complex. The results showed an increase of complexation with increasing temperature resulting in both a positive molal enthalpy ($\Delta_R H^\circ_m$) and entropy ($\Delta_R S^\circ_m$) of reaction.

In the present study, we have extended the range of $-\log_{10}$ [H^+] from 2.52 up to 3.65. This increases the amounts of $H_2PO_4^-$ and HPO_4^{2-} in solution and subsequently the possibility for the formation of the $Cm(H_2PO_4)_2^+$, $Cm(H_2PO_4)_3^0$, and/or $Cm(HPO_4)^+$ complexes. Namely, one can gain an insight into the Cm(III)−phosphate speciation as a function of pH and total phosphate concentration under conditions where solid Cm(III)−phosphate precipitation can be avoided. The complexation studies were conducted at several ionic strengths (I = 0.5−3.0 mol·L^{-1} $NaClO_4$) to allow for the use of the SIT approach for the extrapolation of the conditional $\log_{10}$ β to infinite dilution and to extract ion interaction parameters (ε) for the found species. In addition, temperature-dependent studies were conducted at $-\log_{10}$ [H^+] = 2.52 from 25 up to 90 °C at I = 1.0 mol·L^{-1} to extract molal enthalpy and entropy of reaction for the Cm(III)−phosphate species present in solution using the integrated van't Hoff equation.

To understand the underlying reasons for the increased stability of the Cm−phosphate complexes at elevated temperature, such as changes in the first-shell coordination, spectroscopic data has been evaluated and compared to *ab initio* simulations of the electronic states of these solution species in 9-fold and 8-fold coordination. Electronic ground-state calculations were used for a qualitative description of the energetic stabilities of the various solution species at different temperatures, while the computations of electronic excited states have been used to link the observed luminescence features with the stoichiometry of the complexes and the first-shell coordination around the Cm^{3+} cation.

2. MATERIALS AND METHODS

2.1. Sample Preparation. *2.1.1. Reagents.* All solutions used in the present study were prepared from high-purity reagent-grade materials without further purification or treatment. $NaClO_4·H_2O$ (Sigma-Aldrich, p.a., ACS reagent, ≥99.5%) and orthophosphoric acid (85% from Merck, Suprapur) were used as the background electrolyte and phosphate source in the samples, respectively. For the dilution of all solutions to the desired concentrations, doubly deionized water (MilliQ) was used. As the curium source, a 1.15 ± 0.1 × 10^{-5} mol·L^{-1} ^{248}Cm stock solution in 0.01 mol·L^{-1} $HClO_4$ was applied. The concentration of this stock solution was determined by liquid scintillation counting (PerkinElmer Tri-Carb 3100TR), taking into account the isotopic composition of the stock solution. Note: ^{248}Cm is a radionuclide with a half-life of 3.48 × 10^5 years, decaying through α-emission (92%) and spontaneous fission (8%). The use of ^{248}Cm requires the appropriate infrastructure and personnel trained in the handling of α-emitting isotopes. All pH-adjustments were conducted with 0.5−5.0 mol·L^{-1} $HClO_4$ (Sigma-Aldrich, p.a) and 2.0−5.0 mol·L^{-1} NaOH (Carl Roth, ≥99%) solutions.

2.1.2. Cm(III)−Phosphate Samples. To account for the Cm(III) speciation at 25 °C in the presence of aqueous phosphates, investigations were conducted at different pH values and ionic strengths. Due to the very low solubility of reported actinide or lanthanide phosphates such as crystalline $LnPO_4·0.667H_2O$ rhabdophane (Ln = La to Dy) with $\log_{10}$ K°_{sp} (25 °C) ranging from −25.6 ± 0.8 (Pr) to −24.9 ± 1.7 (Eu)[24] and amorphous $AmPO_4·xH_2O$ with $\log_{10}$ K°_{sp} (25 °C) = −24.79 ± 0.18,[25] the first set of experiments were conducted at rather acidic conditions of $-\log_{10}$ [H^+] = 2.52. At this pH value and ionic strengths of 0.5, 1.0, and 2.0 mol·L^{-1}, the solubility product of Cm−rhabdophane will not be exceeded for total Cm(III) concentrations of 8.76 × 10^{-8}−1.15 × 10^{-7} mol·L^{-1} and total phosphate concentrations [$\Sigma(PO_4)$] up to 0.055 mol·L^{-1} used in the experiments. At this low pH, however, the phosphate speciation is dominated by the $H_2PO_4^-$ ligand, while the overall HPO_4^{2-} concentration, even in the samples with 0.055 mol·L^{-1} phosphate remains very low, at approximately 3 × 10^{-6} mol·L^{-1}. Therefore, in order to increase the amount of HPO_4^{2-} in solution, a second set of experiments were conducted at a higher pH of $-\log_{10}$ [H^+] = 3.44 (I = 1.0 and 2.4 mol·L^{-1}) or 3.65 (I = 3.0 mol·L^{-1}). In these experiments, the overall curium concentration was decreased to 1.15 × 10^{-8} mol·L^{-1} to suppress the formation of Cm−rhabdophane, while the total phosphate concentration was kept below 0.08 mol·L^{-1}.

All the abovementioned samples, independent of the pH, were prepared by mixing $NaClO_4$ and H_3PO_4 to the desired overall ionic strength and phosphate concentrations, respectively. Thereafter, the sample pH was adjusted by adding appropriate amounts of either $HClO_4$ or NaOH to the samples. The measured pH (pH_{exp}) was corrected for ionic strength effects using eq 1 to obtain the actual molar H^+ concentration.

$$-\log_{10}[H^+] = pH_{exp} + A_c \quad (1)$$

The coefficient A_c was determined based on eq 2 derived in our previous study from solutions with known H^+ concentrations at different ionic strengths imposed by $NaClO_4$ (0.5 to 4 mol·L^{-1}),[14] where I is the ionic strength in mol·L^{-1}.

$$A_c = 0.0127 \times I^2 + 0.1568 \times I + 0.0606 \quad (2)$$

The pH measurements were done with combination pH electrodes (SenTix MIC from VWR) taking into account the different A_c coefficients for the samples prepared at different ionic strengths. In order to avoid precipitation of $KClO_4$ in the diaphragm of the electrode, the original junction electrolyte (3 mol·L^{-1} KCl) was replaced by 3 mol·L^{-1} NaCl solution (Carl Roth, ≥99.5%). The electrodes were calibrated using standard buffer solutions (certified to PTB/NIST) with pH values of 1.679 ± 0.02 and 4.006 ± 0.02 (WTW). After an equilibration time of at least 1 day, the sample pH was remeasured and readjusted if necessary followed by addition of 5−50 μL of Cm(III) stock solution to the samples. After Cm(III) addition, no additional pH adjustment was undertaken to avoid rhabdophane precipitation as a result of NaOH addition to the samples. The final curium and phosphate concentrations as well as the ionic strength in the samples were calculated based on the added amount of background electrolyte and the added volumes of acids and bases during the pH adjustments. No separate determination of the curium or phosphate concentrations in the individual samples was conducted.

To investigate the impact of elevated temperature on the Cm(III)−phosphate complexation reaction, the solutions prepared at I = 1.0 mol·L^{-1} and $-\log_{10}$ [H^+] = 2.52 were taken and stepwise heated up to 90 °C using an HLCThermoMixer (MKR 23 BlockThermostate, Ditabis). All experimental conditions are summarized in Table 2.

2.2. Speciation Calculations. The determination of the complexation constants via slope analysis requires the molality of free H_3PO_4, which was calculated using the geochemical speciation software PHREEQC.[26] The activity coefficients were treated by the

https://doi.org/10.1021/acs.inorgchem.1c01319
Inorg. Chem. 2021, 60, 10656−10673

Table 2. Overview of the Experimental Conditions Used in the Various Cm(III)−Phosphate Complexation Rows

$-\log_{10}[H^+]$	I (mol·L^{-1})	T (°C)	[Cm(III)] (mol·L^{-1})	$[\Sigma(PO_4)]_{max}$ (mol·L^{-1})
2.52	0.5	25	1.15×10^{-7}	0.055
2.52	2.0	25	8.76×10^{-8}	0.04
2.52	1.0	25−90	1.15×10^{-7}	0.055
3.44	1.0	25	1.15×10^{-8}	0.070
3.44	2.4	25	1.15×10^{-8}	0.08
3.65	3.0	25	1.15×10^{-8}	0.040

SIT approach using the ThermoChimie dataset (version 9b0) from Andra.[27] All calculations were performed in the molal scale with chemical conditions (ionic strength, total phosphate molality, $-\log_{10} m_{H^+}$, and temperature) identical to those applied in the experiments. The conversion from the molar to the molal scale was done using the density of $NaClO_4$ reported by Söhnel and Novotný.[28]

2.3. Luminescence Spectroscopy. Luminescence spectroscopy was used to study the complexation reaction between Cm(III) and phosphates. After addition of Cm(III) to the phosphate-containing samples, measurements were undertaken within a day to avoid sample aging and the possibility of rhabdophane precipitation over time. For the luminescence spectroscopic measurements, 3 mL of the sample was transferred into a quartz glass cuvette with a PTFE stopper. To ensure complete tightness of the cuvettes during the high-temperature measurements, a semitransparent, thermoplastic film was wrapped around the cuvette stoppers and exchanged if necessary. The desired temperature was achieved by pre-equilibrating the samples in block thermostats (HLCThermoMixer, MKR 23 Ditabis) followed by an additional equilibration time of at least 10 min in a heatable cuvette holder with a temperature control accuracy of ±0.05 °C. The luminescence spectroscopic investigations were conducted with a dye laser setup (NarrowScan, Radiant Dyes), coupled to a Nd:YAG (Continuum, Surelite) pump laser. The dye consisted of a 1:1 mixture of Exalite 389 and Exalite 398. Cm(III) luminescence emission spectra were recorded between 570 and 615 nm (1200 lines·mm^{-1}, Cm(III)−phosphate rows at $-\log_{10}[H^+] = 2.52$) or 560 and 630 nm (600 lines·mm^{-1}, Cm(III)−phosphate rows at $-\log_{10}[H^+] = 3.44$−3.65), 1 μs after the exciting laser pulse with a constant excitation wavelength of 396.6 nm. Thus, the respective wavelength resolutions achieved in the measurements were 0.18 and 0.25 nm. The laser pulse energy was measured by a pyroelectric energy sensor and was found to be between 3 and 5 mJ in each measurement. Luminescence emission was detected by an optical multichannel analyzer (Shamrock 303i) and an ICCDCamera (iStar, Andor). Luminescence lifetime measurements were collected for selected samples, by recording the luminescence emission as a function of delay time between the laser pulse and the camera gating. A delay increment between 5 and 7 μs was used for an overall delay time of 260 μs.

The collected luminescence data was treated with the programs Matlab[29] (2019, version 2) and OriginPro[30] (version 2019). Matlab was used to integrate the collected luminescence emission spectra as a function of delay time to obtain luminescence lifetime decay curves. Origin was used for the stepwise extraction of pure component spectra from the measured composite spectra. The calculation of the Cm(III)−phosphate species distribution was done with MS Excel using a least squares fitting method described in detail in Huittinen et al.[31] and Eibl et al.[32] Luminescence intensity (LI) factors for the correction of relative luminescence intensity variations of the present species were measured by comparing the intensity of the uncomplexed Cm(III) aqua ion with the measured Cm(III)−phosphate spectra and by fitting the LI factors using the same least squares fit approach. Eventually, the obtained pure component spectra (aqua ion and Cm(III)−phosphate complexes) were fitted with four Lorentzian peaks describing the emission from the four crystal field states (denoted A_1−A_4 by convention) of the emitting electronic level back to the ground state. For the fit, the area under the peak (population of the crystal field levels) was constrained to follow the Boltzmann distribution given by eq 3.

$$\frac{N_f}{N_i} = \exp\left(-\frac{\Delta E}{k_B T}\right) \tag{3}$$

N_f and N_i refer to the population of the various crystal field levels of the excited state and the ground state, respectively. ΔE is the band gap between the excited state and the ground state ($\Delta E = hc\left(\frac{1}{\lambda_f} - \frac{1}{\lambda_i}\right)$, h = Planck constant (6.62607×10^{-34} J·s), c = the speed of light in vacuum (2.99792×10^8 m·s^{-1}), and λ = emission wavelength in meters), T is the temperature in Kelvin, and k_B is the Boltzmann constant (1.38065×10^{-23} J·K^{-1}). To reduce the number of free variables in the fit, the FWHM of two consecutive transitions was constrained to follow FWHM (A_{n+1}) ≥ FWHM (A_n), n = 1−3.

The fitted peak positions were thereafter used to compare the experimental crystal field splitting with the computed ones, as explained in more detail later in the text (Section 3.3).

2.4. *Ab Initio* Simulations. In the present study, *ab initio* simulations were conducted to (i) investigate the chemical bond properties as a function of the number of ligands and (ii) to shed light on the spectroscopic properties by means of excited-state electronic structure calculations. With this aim, the geometries of the various species involved in the complexation processes, *i.e.*, $H_2PO_4^-$, H_3PO_4, $[Cm(H_2O)_{8,9}]^{3+}$, $[Cm(H_2O)_{7,8}(H_2PO_4)]^{2+}$, and $[Cm(H_2O)_{6,7}(H_2PO_4)_2]^+$ were optimized. The appropriate thermodynamic corrections including enthalpy, entropy, solvent effects, and the spin−orbit coupling contributions to estimate the Gibbs free energy values of the complexation reactions were applied. For each Cm-containing species, the absorption and emission transitions were computed.

2.4.1. Structures, Bonding Analysis, Thermodynamic Corrections, and Solvent Correction. The structures used for the H_2O, $H_2PO_4^-$, H_3PO_4, $[Cm(H_2O)_{8,9}]^{3+}$, $[Cm(H_2O)_{7,8}(H_2PO_4)]^{2+}$, and $[Cm(H_2O)_{6,7}(H_2PO_4)_2]^+$ species were optimized using the second-order Møller−Plesset perturbation theory (MP2) and Unrestricted MP2 (UMP2) methods for the open-shell systems combined with Resolution of the Identity[33,34] with the appropriate atomic auxiliary basis functions.[35,36] For the Cm(III) complexes, a high-spin octet state was considered by occupying the seven 5f orbitals of the Cm(III) cation by the seven unpaired electrons. Relativistic small-core pseudopotentials (60 e^- in core) of the Stuttgart−Cologne group were employed, associated with the def2-TZVP basis sets (14s13p10d8f)/[10s9p5d4f3g] for the Cm(III) cation.[37] Identical basis sets quality was considered for the lighter elements in all molecules.[38]

To analyze the nature of the curium−ligand chemical bonds, the quantum theory of atoms-in-molecules (QTAIM) analysis was applied. In this context, the Gaussian 16 (Revision B01) quantum chemistry package[39] with the same basis sets was used to generate the appropriate wave-function extended files (wfx) to be used by the AIMAll package.[40] To estimate harmonic vibrational partition functions at 25 and 90 °C and 0.1 MPa, which are necessary to calculate the enthalpic and entropic contributions to the gas-phase energies, numerical frequency calculations were also performed.

The Conductor-like Screening Model (COSMO)[41] was used to represent implicitly water as polarizable dielectric continuum and make it possible to estimate the solvation Gibbs free energies at the two different temperatures using two dielectric constants for the water solvent ε_r = 78 at 25 °C and ε_r = 58 at 90 °C. All the calculations were performed with the Turbomole 7.4.1 package.[42,43]

2.4.2. Predictions of the Ground-State Energies and Spectroscopic Calculations. To derive the most accurate ground-state energies of Cm(III) complexes and to compute the transition energies of the excited states, state-averaged CASSCF (complete-active-space self-consistent field) scalar relativistic calculations with the Douglas−Kroll−Hess Hamiltonian[44,45] were performed for all the possible multiplicities encountered for seven unpaired 5f electrons, i.e., 1 octet, 48 sextet, 392 quartet, and 784 doublet states. Spin−orbit coupling

https://doi.org/10.1021/acs.inorgchem.1c01319
Inorg. Chem. 2021, 60, 10656−10673

contributions to the gas-phase energies were computed with the Restricted Active Space State Interaction (RASSI) approach,[46] by coupling all CASSCF wave functions, while dynamical correlation contributions to the ground-state energies were accounted for with the XMS-CASPT2 approach (multistate complete active space second-order perturbation theory) only for Cm(III) complexes as light molecules are treated with the single-reference MP2 method. In the MP2 and XMS-CASPT2 calculations, the 1s core orbitals of the oxygen atoms and up to the 5s, 5p, and 5d orbitals of the actinide ions were kept frozen. Absorption and emission energies were computed shifting the energy of the excited states obtained at the SO-CASSCF level, by a quantity that corresponds to the spin-free energy difference of the first sextet state obtained at the CASSCF and XMS-CASPT2 levels. Note that it was impossible to perform XMS-CASPT2 calculations for the other multiplicities (quartets and doublets) as the states were too numerous. All HF/CASSCF and MP2/XMS-CASPT2 ground-state energies were extrapolated to the Complete Basis Set limit (CBS limit), from calculations using the all-electron Atomic Natural Orbital relativistic core correlation (ANO-RCC) basis sets optimized by Roos et al.[47,48] with triple-zeta and quadruple-zeta basis sets, and applying two-point extrapolation formulas.[49−51] These relativistic wave-function calculations were performed with the OpenMolcas program.[52,53]

2.4.3. Composite Method for Thermodynamic Estimations and Chemical Reactions. To estimate the $\Delta G_r^\circ(T)$ for the following reactions (n = 9)

$$[Cm(H_2O)_n]^{3+} \rightarrow [Cm(H_2O)_{n-1}]^{3+} + H_2O \quad (R1)$$

$$[Cm(H_2O)_{n-1}(H_2PO_4)]^{2+} \rightarrow [Cm(H_2O)_{n-2}(H_2PO_4)]^{2+} + H_2O \quad (R2)$$

$$[Cm(H_2O)_{n-2}(H_2PO_4)_2]^{+} \rightarrow [Cm(H_2O)_{n-3}(H_2PO_4)_2]^{+} + H_2O \quad (R3)$$

one has to determine the Gibbs free energy associated with each reactant and product by adding all contributions listed below.

$$G(A, T) = E^{CBS}_{XMS-CASPT2}(A) + E^{SO}(A) + G^{gaz}_{coor}(A, T) + G^{sol}(A, T)$$

For a compound A, these contributions encompass the CBS extrapolated scalar relativistic electronic energy ($E^{CBS}_{XMS-CASPT2}(A)$), the spin−orbit contribution $E^{SO}(A)$ for the Cm(III) complexes, Gibbs free energy correction $G^{gaz}_{coor}(A, T)$, and the hydration Gibbs free energy $G^{sol}(A, T)$. Note that for all these reactions listed above, a correction of RT ln(55.34) needs to be added to account for the change of the standard state for the released water molecule from pure water (concentration of 55.34 mol·L^{-1}) to the reference standard state 1 mol·L^{-1}.[54]

3. RESULTS

3.1. Influence of pH and Ionic Strength on Cm(III) Complexation with Phosphate at 25 °C. *3.1.1. Luminescence Spectroscopy.* Cm(III) (1.15×10^{-7} mol·L^{-1}) luminescence emission spectra collected from phosphate-containing solutions with $[\Sigma(PO_4)]$ ranging from zero to 0.055 mol·L^{-1} at 25 °C, $-\log_{10}[H^+]$ = 2.52, and I = 1.0 mol·L^{-1} are presented in Figure 1, top, left. The data corresponding to $[Cm(III)] = 1.15 \times 10^{-8}$ mol·L^{-1}, $[\Sigma(PO_4)]_{max}$ = 0.07 mol·L^{-1}, and I = 1.0 mol·L^{-1} at a lower proton concentration of $-\log_{10}[H^+]$ = 3.44 is presented in Figure 1 top, right.

Both sets of recorded luminescence spectra show a clear shift toward longer wavelengths with increasing phosphate concentration, pointing toward a progressing complexation reaction in solution between Cm(III) and the phosphate ligands. To obtain the pure component spectra of the individual species as well as their relative distributions and luminescence intensity factors, the measured multicomponent spectra were decomposed as explained in Section 2.3. At a higher proton concentration of $-\log_{10}[H^+]$ = 2.52, two components in addition to the noncomplexed Cm(III) aqua ion could be obtained (Figure 1, bottom, left). The peak positions of the two Cm(III)−phosphate complexes are found at 599.2 and 600.4 nm. The former spectrum is identical, both in terms of the peak position and the overall peak shape, to the one obtained in our previous study for the $Cm(H_2PO_4)^{2+}$ complex.[14] Thus, the first Cm−phosphate species obtained in the present study can be assigned to the 1:1 (Cm^{3+}:$H_2PO_4^-$) $Cm(H_2PO_4)^{2+}$ species. The second species, however, may arise either from additional complexation of Cm with the $H_2PO_4^-$ ligand resulting in, *e.g.*, a 1:2 complex ($Cm(H_2PO_4)_2^+$) or from complexation with HPO_4^{2-}, resulting in $Cm(HPO_4)^+$. By increasing the solution pH, an additional Cm(III)−phosphate complex can be identified from the decomposed luminescence spectra with a peak maximum at 601.9 nm (Figure 1, bottom, right). The signal-to-noise ratio of the obtained spectrum is very low, owing to the very low amount of this species in solution. As this third species is not present in the lower pH regime for comparable phosphate concentrations, we tentatively assign the species to the $Cm(HPO_4)^+$ complex. Subsequently, the aforementioned Cm(III)−phosphate species, also present at lower pH, is likely to be the $Cm(H_2PO_4)_2^+$ complex. A detailed discussion of the phosphate speciation and the stoichiometries of the derived complexes will be given in Section 3.1.2.

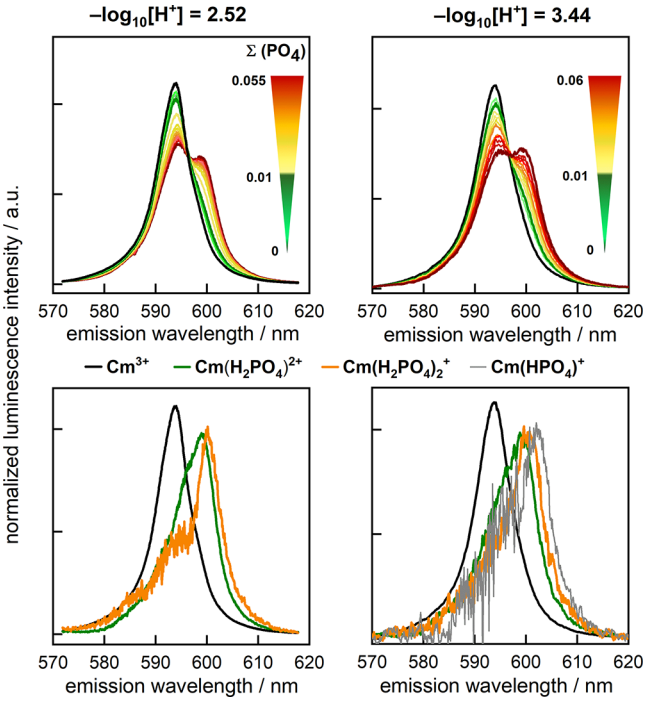

Figure 1. Top: Cm(III) luminescence emission spectra at 25 °C, I = 1.0 mol·L^{-1} in the presence of $\Sigma(PO_4)$ = 0−0.055 mol·L^{-1} at $-\log_{10}[H^+]$ = 2.52 (left) and $[\Sigma(PO_4)]$ = 0−0.07 mol·L^{-1} at $-\log_{10}[H^+]$ = 3.44 (right). Bottom: pure component spectra for the Cm(III) aqua ion and various Cm(III)−phosphate complexes.

From the obtained pure component spectra, the relative distributions of the individual species were calculated, taking into account the different luminescence quantum yields of the species relative to the aqua ion (LI factors). The corrected species distributions using LI factors of 1.00 for the aqua ion and 0.89 ± 0.14, 0.97 ± 0.22, and 1.15 ± 0.62 for the

https://doi.org/10.1021/acs.inorgchem.1c01319
Inorg. Chem. 2021, 60, 10656−10673

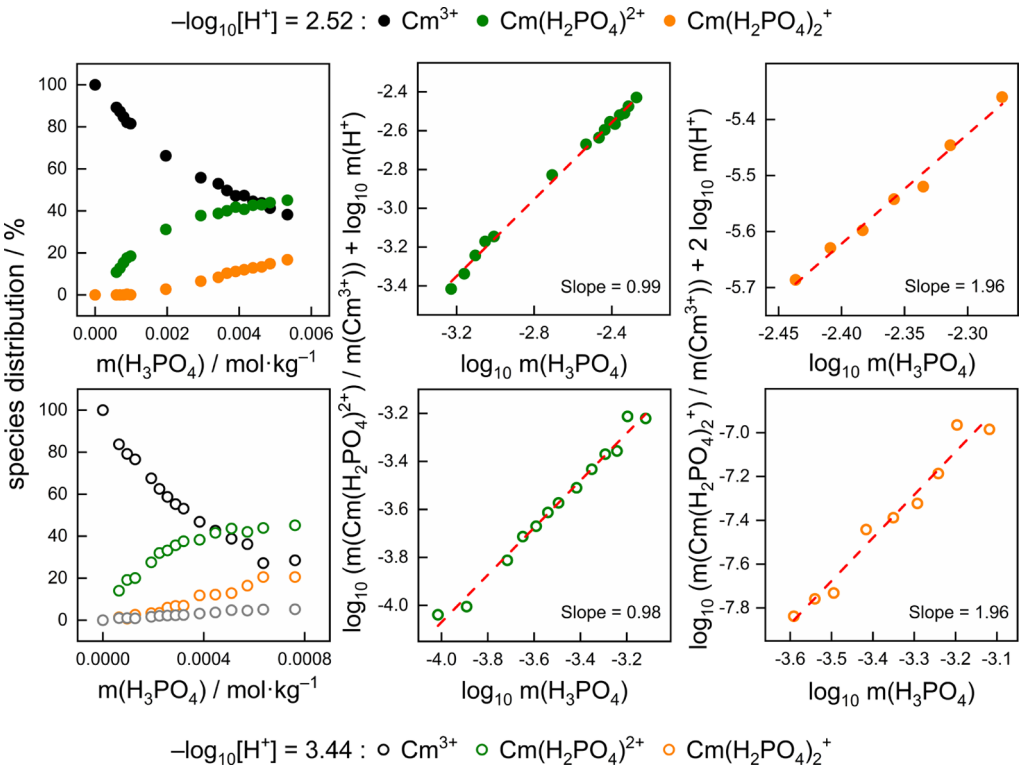

Figure 2. Cm(III) species distribution at 25 °C, I = 1.0 mol·L^{-1} in the presence of [Σ(PO_4)] = 0−0.055 mol·L^{-1} at −log$_{10}$ [H$^+$] = 2.52 (top, left) and [Σ(PO_4)] = 0−0.07 mol·L^{-1} at −log$_{10}$ [H$^+$] = 3.44 (bottom, left). The corresponding slope analyses obtained from the species distributions are shown for species 1 ($Cm(H_2PO_4)^{2+}$), middle, and species 2 ($Cm(H_2PO_4)_2^+$), right.

phosphate complexes 1 ($Cm(H_2PO_4)^{2+}$), 2 ($Cm(H_2PO_4)_2^+$), and 3 ($Cm(HPO_4)^+$), respectively, are presented in Figure 2 for −log$_{10}$ [H$^+$] = 2.52 (top, left) and −log$_{10}$ [H$^+$] = 3.44 (bottom, left). Species distributions for other ionic strengths at the two investigated pH values are available in Figure S1 in the Supporting Information.

As expected, the amount of Cm(III)−phosphate complexes is slightly higher at −log$_{10}$ [H$^+$] = 3.44 than at −log$_{10}$ [H$^+$] = 2.52. In addition, the third Cm(III)−phosphate complex ($Cm(HPO_4)^+$) is only present at the higher pH value in the investigated phosphate concentration range. The reason for the enhanced phosphate-complex formation with increasing pH can be attributed to the increasing amounts of $H_2PO_4^-$ and HPO_4^{2-} ligands in solution as the phosphoric acid (H_3PO_4) dissociates. In agreement with our previous study, an increase of the ionic strength leads to a slight increase of the amount of Cm(III)−phosphate complexes in solution (see Figure S1). The derivation and the magnitude of the Cm(III)−phosphate complexation constants will be discussed in Section 3.1.2.

Luminescence lifetimes (τ), which can provide information on the number of coordinating water molecules around the Cm(III) cation using (eq 4) proposed by Kimura and Choppin,[55] were collected for selected samples at both investigated pH values.

$$n(H_2O) = \frac{0.65}{\tau(\text{ms})} - 0.88 \tag{4}$$

The obtained lifetime curves (the natural logarithm of the integrated luminescence intensity vs delay time between the laser pulse and camera gating) all decay monoexponentially despite the presence of at least two components in all measured samples (see Figure S2). This implies that the dynamic exchange reactions in the Cm(III) hydration sphere between coordinated water and phosphate ligands occur faster than the luminescence decay of the individual species. In order to draw a conclusion on the coordination of the phosphate ligands via the amount of coordinating water around the Cm(III) ion in solution, theoretical lifetimes were calculated according to eq 5, assuming lifetimes of 68 μs for the Cm(III) aqua ion (9 H_2O), 73 μs for $Cm(H_2PO_4)^{2+}$ (8 H_2O), and 83 μs for $Cm(H_2PO_4)_2^+$ and $Cm(HPO_4)^+$ (7 H_2O).

$$\frac{1}{\tau(\text{calc.})} = a \times \frac{1}{68\ \mu s} + b \times \frac{1}{73 \mu s} + (c + d) \times \frac{1}{83\ \mu s} \tag{5}$$

The factors a−d are the fractions of the individual species determined from the experimentally derived species distributions (noncorrected for relative differences in the luminescence quantum yield). The reported uncertainties for the factors include the error resulting from the decomposition of the spectra and the subsequent fits yielding the tabulated fractions. These assumed lifetimes imply monodentate coordination of the $H_2PO_4^-$ ligand, where each coordinated ligand replaces one H_2O in the first hydration sphere and bidentate coordination of HPO_4^{2-} resulting in the replacement of two H_2O around the Cm(III) cation. The results of the experimental fits and the calculated lifetimes are summarized in Table 3.

At a first glance, the experimental and theoretical values are in very good agreement with one another. This would imply that the assumed coordination of the phosphate ligands to the Cm(III) cation follows the denticity proposed above, i.e., monodentate to the $H_2PO_4^-$ ligand and bidentate to HPO_4^{2-}. The denticity to the latter ligand, however, should be

https://doi.org/10.1021/acs.inorgchem.1c01319
Inorg. Chem. 2021, 60, 10656−10673

Table 3. Experimentally Determined and Calculated Luminescence Lifetimes of Cm(III)−Phosphate Solutions at 25 °C

$-\log_{10}[H^+]$	$[\Sigma(PO_4)]$ (mol·L^{-1})	derived fractions (a–d) of Cm(III) species[a]	τ(exp.) (μs)	τ(calc.) (μs)
2.52	0.009	a = 0.83 ± 0.04, b = 0.17 ± 0.01	68 ± 2	69
2.52	0.02	a = 0.66 ± 0.05, b = 0.29 ± 0.02, c = 0.05 ± 0.01	70 ± 2	70
2.52	0.045	a = 0.43 ± 0.03, b = 0.41 ± 0.03, c = 0.16 ± 0.01	71 ± 2	72
3.44	0.02	a = 0.57 ± 0.05, b = 0.33 ± 0.04, c = 0.07 ± 0.02, d = 0.03 ± 0.01	71 ± 3	71
3.44	0.04	a = 0.38 ± 0.04, b = 0.42 ± 0.05, c = 0.13 ± 0.02, d = 0.07 ± 0.01	73 ± 2	73
3.44	0.06	a = 0.27 ± 0.03, b = 0.43 ± 0.05, c = 0.22 ± 0.03, d = 0.08 ± 0.01	76 ± 3	74

[a] $a(Cm^{3+})$, $b(Cm(H_2PO_4)^{2+})$, $c(Cm(H_2PO_4)_2^+)$, $d(Cm(HPO_4)^+)$, $a + b + c + d = 1$.

considered merely hypothetical due to the very low amount of the presumed $Cm(HPO_4)^+$ species in the samples, subsequently having only a small influence on the luminescence lifetimes. Due to the uncertainties of the experimentally determined lifetimes in combination with the very moderate changes of the lifetimes as a result of phosphate complexation where only one or two water molecules are removed from the Cm(III) hydration sphere, computational studies were performed to support these conclusions (see Section 3.3).

*3.1.2. Determination of the Conditional $\log_{10}$ *β and $\log_{10}$ *β^0 at 25 °C. 3.1.2.1. Determination of the Conditional Complexation Constants at 25 °C.* From the deconvolution of the luminescence spectra at the different $-\log_{10}[H^+]$ and ionic strengths investigated at 25 °C, the molar concentrations of the Cm^{3+} aqua ion and the $Cm(H_2PO_4)^{2+}$ and $Cm(H_2PO_4)_2^+$ complexes could be obtained. These concentrations were at first converted to the molal scale using the density of $NaClO_4$, the background electrolyte, reported by Söhnel and Novotný.[28] These molalities were used to calculate the conditional complexation constants $\log_{10}$ *β assuming the two following equilibria:

$$Cm^{3+} + H_3PO_4 \rightleftharpoons Cm(H_2PO_4)^{2+} + H^+,\ \log_{10}{}^*\beta_1 \quad (R4)$$

$$Cm^{3+} + 2H_3PO_4 \rightleftharpoons Cm(H_2PO_4)_2^+ + 2H^+,\ \log_{10}{}^*\beta_2 \quad (R5)$$

The asterisk is used here to represent a complexation reaction involving the deprotonation of the H_3PO_4 ligand.[21]

In all experiments, the molality of Cm(III) was orders of magnitude lower than the one of phosphoric acid. Thus, one can assume that the speciation of the different phosphate ligands was not significantly impacted by the complexation with Cm(III). By applying the law of mass action, the following expressions of the conditional complexation constant were obtained:

$$\log_{10}{}^*\beta_1 = \log_{10}\left(\frac{m_{Cm(H_2PO_4)^{2+}}\cdot m_{H^+}}{m_{Cm^{3+}}\cdot m_{H_3PO_4}}\right) \quad (6)$$

$$\log_{10}{}^*\beta_2 = \log_{10}\left(\frac{m_{Cm(H_2PO_4)_2^+}\cdot (m_{H^+})^2}{m_{Cm^{3+}}\cdot (m_{H_3PO_4})^2}\right) \quad (7)$$

Based on eqs 6 and 7, the terms $\log_{10}\frac{m_{Cm(H_2PO_4)^{2+}}}{m_{Cm^{3+}}} + \log_{10} m_{H^+}$ and $\log_{10}\frac{m_{Cm(H_2PO_4)_2^+}}{m_{Cm^{3+}}} + 2\log_{10} m_{H^+}$ were exemplarily plotted as a function of $\log_{10} m_{H_3PO_4}$ at an ionic strength of 1 mol·L^{-1} (Figure 2, middle and right). The results of the slope analysis for all other conditions are given in Figure S3 for $Cm(H_2PO_4)^{2+}$ and Figure S4 for $Cm(H_2PO_4)_2^+$. The slopes were systematically close to 1 and 2, respectively, confirming the postulated formation of the $Cm(H_2PO_4)^{2+}$ and $Cm(H_2PO_4)_2^+$ complexes. Note that the individual slopes were just aiming at verifying the stoichiometry of the proposed complexes and were not used for the derivation of the conditional complexation constants. For the second Cm−phosphate species, the formation of $Cm(HPO_4)^+$ based on the following equilibrium

$$Cm^{3+} + H_3PO_4 \rightleftharpoons Cm(HPO_4)^+ + 2H^+$$

was also considered but eventually not retained. Indeed, the slope analysis led to a slope of 2 (Figure 2, right) and not 1.

At constant m_{H^+} and ionic strength, a conditional complexation constant was calculated at each phosphate concentration using the law of mass action. These values were averaged and correspond to the conditional $\log_{10}$ *β summarized in Table 4.

Table 4. Thermodynamic Conditional Complexation Constants for the Formation of $Cm(H_2PO_4)^{2+}$ and $Cm(H_2PO_4)_2^+$ at 25 °C at Varying Ionic Strengths ($\log_{10}$ *β in the Molal Scale)

ionic strength (mol·L^{-1})	ionic strength (mol·kg^{-1})	$-\log[H^+]$	$\log_{10}{}^*\beta_1$	$\log_{10}{}^*\beta_2$
0.5	0.51	2.52	−0.20 ± 0.10	−0.87 ± 0.15
0.6	0.62	1.00	−0.25 ± 0.22[a]	
1.0	1.05	2.52	−0.16 ± 0.15	−0.82 ± 0.25
1.0	1.05	3.44	−0.08 ± 0.15	−0.68 ± 0.25
1.1	1.16	1.00	−0.14 ± 0.10[a]	
2.0	2.21	2.52	−0.13 ± 0.15	−0.57 ± 0.30
2.1	2.33	1.00	−0.06 ± 0.11[a]	
2.4	2.71	3.44	0.02 ± 0.20	−0.57 ± 0.35
3.0	3.50	3.65	0.05 ± 0.20	−0.43 ± 0.40

[a] Values were taken from Jordan et al.[14]

The highest standard deviation for the $\log_{10}$ *β obtained within all experiments in this study was 0.07. However, one can see that the uncertainties in Table 4 are higher, and the underlying reason will be explained. As already mentioned by Jordan et al.,[14] the SIT database from ThermoChimie suffers from a conflict between the ion interaction model and the ion association model. Indeed, the ThermoChimie database contains both complexation constants for the formation of several ion pairs between Na^+ and the phosphate ligands, i.e., $NaH_2PO_4^0$, $Na(HPO_4)^-$, and $NaPO_4^{2-}$ as well as the $\varepsilon(Na^+;H_2PO_4^-)$, $\varepsilon(Na^+;HPO_4^{2-})$, and $\varepsilon(Na^+;PO_4^{3-})$ ion interaction coefficients. Resolving this contradiction needs efforts that would exceed the scope of this work. Consequently, all molalities of the free H_3PO_4 were calculated one more time without considering the formation of these three ion pairs, and the respective conditional complexation constants $\log_{10}$ *β (no

https://doi.org/10.1021/acs.inorgchem.1c01319
Inorg. Chem. 2021, 60, 10656−10673

ion pairs) were derived. Eventually, a pragmatic approach was used, i.e., the uncertainties of the conditional complexation constants $\log_{10}$ *β summarized in Table 4 (calculated using the raw SIT Thermochimie database) were increased to allow an overlap with the complexation constants $\log_{10}$ *β (no ion pairs) (obtained without considering the formation of the $NaH_2PO_4^0$, $Na(HPO_4)^-$, and $NaPO_4^{2-}$ ion pairs).

According to Table 4, increasing the ionic strength at constant $[H^+]$ or decreasing the $[H^+]$ at constant ionic strength leads to an increase of the conditional complexation constants derived at 25 °C for both $Cm(H_2PO_4)^{2+}$ and $Cm(H_2PO_4)_2^+$ complexes.

3.1.2.2. Extrapolation to Infinite Dilution at 25 °C. The conditional complexation constants were extrapolated to the infinite dilution state applying the SIT equation, in which the basic assumption is that the reactants and products of the reaction only interact with the ions of the background electrolyte. No interaction between species bearing the same charge sign is considered, whereas neutral species are also assumed to not interact with other ions. The activity coefficient of a species j (reactant or product) interacting with species k is expressed as follows

$$\log_{10}\gamma_j = -z_j^2 D + \sum_k \varepsilon(j;\,k)\cdot m_k \tag{8}$$

where z_j stands for the charge of species j, ε(j;k) represents the ion interaction coefficient between species j and species k, m_k is the molality of species k, and D is the Debye–Hückel term:

$$D = \frac{A\cdot\sqrt{I_m}}{1 + Ba_i\cdot\sqrt{I_m}} \tag{9}$$

The term A is the Debye–Hückel constant. According to Grenthe et al.,[21] A = 0.509 $kg^{1/2}\cdot mol^{-1/2}$ at 25 °C, whereas the empirical parameter Ba_i is taken to be 1.5 $kg^{1/2}\cdot mol^{-1/2}$ for all temperatures up to 90 °C.[21]

The relation between the conditional complexation constant and the equilibrium complexation constant at infinite dilution is given by the following equation:

$$\log_{10}{}^*\beta - \Delta z^2 D = \log_{10}{}^*\beta^\circ - \Delta\varepsilon I_m \tag{10}$$

For the two equilibria under consideration (R4 and R5), the following expressions for $\Delta\varepsilon$ are obtained:

$$\Delta\varepsilon = \varepsilon(Cm(H_2PO_4)^{2+};\,ClO_4^-) + \varepsilon(H^+;\,ClO_4^-) - \varepsilon(Cm^{3+};\,ClO_4^-) \tag{11}$$

$$\Delta\varepsilon = \varepsilon(Cm(H_2PO_4)_2^+;\,ClO_4^-) + 2\times\varepsilon(H^+;\,ClO_4^-) - \varepsilon(Cm^{3+};\,ClO_4^-) \tag{12}$$

The interaction coefficient $\varepsilon(H^+;ClO_4^-)$ was taken from Grenthe et al.,[21] while $\varepsilon(Cm^{3+};ClO_4^-)$ was postulated to be equal to $\varepsilon(Am^{3+};ClO_4^-)$ = 0.49 ± 0.03 $kg\cdot mol^{-1}$. Following the SIT formalism, all ion interaction coefficients of the uncharged species H_3PO_4 were set to zero.[21] Δz^2 = Σz^2 (products) − Σz^2 (reactants) were equal to −4 and −6 for reactions R4 and R5, respectively.

By plotting $\log_{10}$ *β − $\Delta z^2 D$ as a function of the ionic strength, a weighted linear regression provided $\log_{10}$ *β° (intercept with the y-axis) and $-\Delta\varepsilon$ (slope) (Figure 3). Detailed explanations on the performance of the weighted linear regression and the derivation of the uncertainties of the

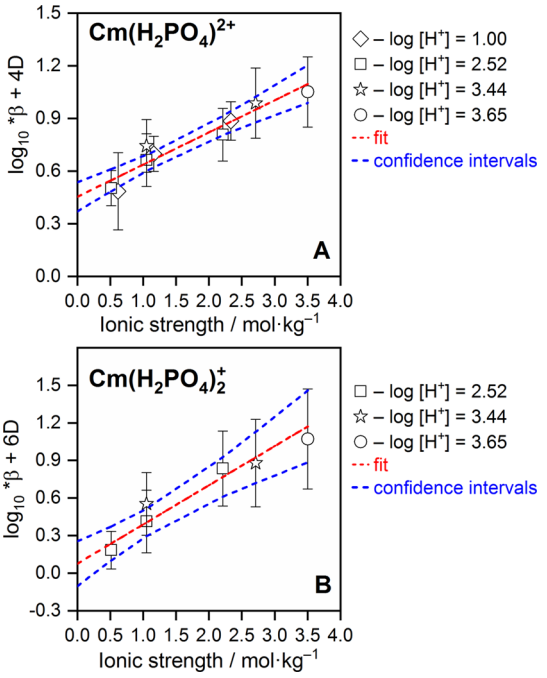

Figure 3. Linear SIT regression plot for the $Cm(H_2PO_4)^{2+}$ (A) and $Cm(H_2PO_4)_2^+$ (B) complexes at 25 °C.

slope and intercept are available elsewhere.[14] However, in the present study, we assumed the individual error variance to be known up to a constant of proportionality k[56] and used the quantiles of the Student's t distribution with n − 2 degrees of freedom to compute the intervals of confidence.

The slopes of the SIT regression for the $Cm(H_2PO_4)^{2+}$ and $Cm(H_2PO_4)_2^+$ complexes were found to be 0.18 ± 0.02 and 0.31 ± 0.04, respectively. The obtained $\log_{10}$ *β° and $\varepsilon(Cm(H_2PO_4)^{2+};ClO_4^-)$ and $\varepsilon(Cm(H_2PO_4)_2^+;ClO_4^-)$ ion interaction coefficients are summarized in Table 5.

Table 5. Complexation Constants at Infinite Dilution ($\log_{10}$ *β°) for the $Cm(H_2PO_4)^{2+}$ and $Cm(H_2PO_4)_2^+$ Complexes and Ion Interaction Coefficients $\varepsilon(Cm(H_2PO_4)^{2+};ClO_4^-)$ and $\varepsilon(Cm(H_2PO_4)_2^+;ClO_4^-)$ at 25 °C

reaction	$\log_{10}$ *β°	$\varepsilon(Cm(H_2PO_4)_n^{(3-n)+};ClO_4^-)$ (kg·mol^{-1})
$Cm^{3+} + H_3PO_4 \rightleftharpoons Cm(H_2PO_4)^{2+} + H^+$	0.45 ± 0.04	0.17 ± 0.04 (n = 1)
$Cm^{3+} + 2H_3PO_4 \rightleftharpoons Cm(H_2PO_4)_2^+ + 2H^+$	0.08 ± 0.07	−0.10 ± 0.06 (n = 2)

The uncertainties on the ion interaction coefficients ε were calculated based on the recommendations in Appendix C in the most recent NEA volume.[21]

$$\sigma_{\varepsilon(Cm(H_2PO_4)^{2+};ClO_4^-)} = \sqrt{(\sigma_{\Delta\varepsilon})^2 + \sigma(\varepsilon(H^+;\,ClO_4^-))^2 + \sigma(\varepsilon(Cm^{3+};\,ClO_4^-))^2} \tag{13}$$

$$\sigma_{\varepsilon(Cm(H_2PO_4)_2^+;ClO_4^-)} = \sqrt{(\sigma_{\Delta\varepsilon})^2 + (2\cdot\sigma(\varepsilon(H^+;\,ClO_4^-)))^2 + \sigma(\varepsilon(Cm^{3+};\,ClO_4^-))^2} \tag{14}$$

https://doi.org/10.1021/acs.inorgchem.1c01319
Inorg. Chem. 2021, 60, 10656−10673

3.2. Influence of Temperature on the Complexation of Cm(III) by Phosphate. *3.2.1. Luminescence Spectroscopy.* For the extraction of thermodynamic data for the two identified complexes, $Cm(H_2PO_4)^{2+}$ and $Cm(H_2PO_4)_2^{+}$, temperature-dependent luminescence spectroscopic measurements were conducted for the sample row prepared at $-\log_{10}[H^+] = 2.52$ and $I = 1.0$ mol·L^{-1} in the temperature range between 25 and 90 °C as explained in Section 2.1.2. Cm(III) emission spectra recorded at two different phosphate concentrations as a function of temperature are presented in Figure S5. Similar to the data collected at 25 °C, a spectral deconvolution of the measured emission spectra was carried out for each temperature, yielding pure component spectra as well as FI-corrected species distributions. The species distribution at 90 °C is presented in Figure 4 (closed symbols), together with the 25 °C data (open symbols).

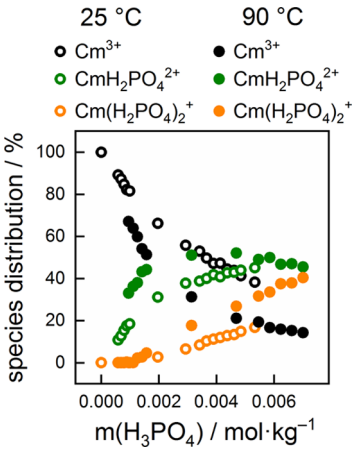

Figure 4. Comparison of the Cm(III) species distribution at 25 and 90 °C in solutions containing 0–0.055 mol·L^{-1} [Σ(PO$_4$)] at $-\log_{10}[H^+] = 2.52$ and $I = 1.0$ mol·L^{-1}.

As evident from both the temperature-dependent Cm(III) emission spectra at constant phosphate concentration (Figure S5) and the obtained species distribution at 90 °C (Figure 4), the complexation reaction between Cm(III) and $H_2PO_4^-$ is promoted with increasing temperature. Only two phosphate complexes, described by similar pure component emission spectra as those obtained at 25 °C, were found over the entire investigated temperature range, speaking for an unchanged Cm(III)–phosphate species present in solution also at elevated temperatures.

*3.2.2. Determination of Conditional Complexation Constants $\log_{10}$ *β at Elevated Temperature and the Thermodynamic Functions $\Delta_R H^\circ_m$ and $\Delta_R S^\circ_m$. 3.2.2.1. Determination of the Conditional Constants at Elevated Temperature.* To determine the molality of the free H_3PO_4 for the slope analysis at elevated temperature, the H^+ molality was assumed to be constant from 25 to 90 °C during the speciation calculations. Indeed, pH measurements up to 80 °C performed in our former study[14] did not reveal significant differences from the pH_{exp} values recorded at 25 °C.

Following the same methodology described above, the terms $\log_{10} \frac{m_{Cm(H_2PO_4)^{2+}}}{m_{Cm^{3+}}} + \log_{10} m_{H^+}$ and $\log_{10} \frac{m_{Cm(H_2PO_4)_2^{+}}}{m_{Cm^{3+}}} + 2 \log_{10} m_{H^+}$ were plotted as a function of $\log_{10} m_{H_3PO_4}$ at an ionic strength of 1 mol·L^{-1} and at 40, 50, 60, 80, and 90 °C (see Figure S6 for $Cm(H_2PO_4)^{2+}$ and Figure S7 for $Cm(H_2PO_4)_2^{+}$). All slopes were close to 1 for $Cm(H_2PO_4)^{2+}$ and close to 2 for $Cm(H_2PO_4)_2^{+}$, indicating no change in the stoichiometry of the formed complexes upon increasing temperature. All resulting conditional $\log_{10}$ *β values for $Cm(H_2PO_4)^{2+}$ and $Cm(H_2PO_4)_2^{+}$ as well as their uncertainties are reported in Tables 6 and 7.

Table 7. Thermodynamic Conditional ($I = 1.0$ mol·L^{-1} at $-\log_{10}[H^+] = 2.52$) and Extrapolated to Infinite Dilution Complexation Constants for the Formation of $Cm(H_2PO_4)_2^{+}$ at Elevated Temperature ($\log_{10}$ *β in the Molal Scale)

temperature (°C)	$\log_{10}$ *β_2	$\log_{10}$ *β_2°
40	−0.78 ± 0.20	0.16 ± 0.20
50	−0.64 ± 0.20	0.33 ± 0.20
60	−0.56 ± 0.20	0.44 ± 0.20
80	−0.38 ± 0.20	0.68 ± 0.20
90	−0.24 ± 0.20	0.85 ± 0.20

Upon increasing the temperature, both equilibria $Cm^{3+} + H_3PO_4 \rightleftharpoons Cm(H_2PO_4)^{2+} + H^+$ and $Cm^{3+} + 2H_3PO_4 \rightleftharpoons Cm(H_2PO_4)_2^{+} + 2H^+$ were shifted toward the product side, resulting in an increase of the conditional complexation constants.

The highest uncertainty for the average $\log_{10}$ *β reported in Tables 6 and 7 was not exceeding 0.02. The same approach

Table 6. Thermodynamic Conditional ($I = 1.1$ mol·L^{-1} at $-\log_{10}[H^+] = 1.00$ and $I = 1.0$ mol·L^{-1} at $-\log_{10}[H^+] = 2.52$) and Extrapolated to Infinite Dilution Complexation Constants for the Formation of $Cm(H_2PO_4)^{2+}$ at Elevated Temperature ($\log_{10}$ *β in the Molal Scale)

temperature (°C)	ionic strength (mol·L^{-1})	$-\log_{10}[H^+]$	$\log_{10}$ *β_1	$\log_{10}$ *β_1°
40	1.1	1.00	−0.12 ± 0.10[a]	0.53 ± 0.10[b]
50	1.1	1.00	−0.08 ± 0.20[a]	0.59 ± 0.20[b]
60	1.1	1.00	−0.02 ± 0.10[a]	0.67 ± 0.10[b]
80	1.1	1.00	0.02 ± 0.10[a]	0.75 ± 0.10[b]
40	1.0	2.52	−0.08 ± 0.10	0.58 ± 0.10
50	1.0	2.52	−0.03 ± 0.10	0.64 ± 0.10
60	1.0	2.52	0.01 ± 0.10	0.70 ± 0.10
80	1.0	2.52	0.15 ± 0.10	0.88 ± 0.10
90	1.0	2.52	0.19 ± 0.10	0.95 ± 0.10

[a]Values were taken from Jordan et al.[14] [b]Uncertainties were recalculated based on the ion interaction coefficient derived in this study.

https://doi.org/10.1021/acs.inorgchem.1c01319
Inorg. Chem. 2021, 60, 10656–10673

described in Section 3.1.2 was applied to reach the final uncertainties reported in Tables 6 and 7.

3.2.2.2. Extrapolation to Infinite Dilution. Similar to the approach used at 25 °C, the conditional complexation constants were extrapolated to infinite dilution applying the SIT equation. At 40 °C (A = 0.523 $kg^{1/2}\cdot mol^{-1/2}$) and 50 °C (A = 0.534 $kg^{1/2}\cdot mol^{-1/2}$), the Debye−Hückel term was taken from the values tabulated by Grenthe et al.[21] At 60, 80, and 90 °C, they were calculated according to Moog and Voigt[57] and were found to be 0.546, 0.571, and 0.585 $kg^{1/2}\cdot mol^{-1/2}$, respectively.

For the extrapolation to infinite dilution, the ion interaction coefficients derived at 25 °C were assumed to be constant in the temperature range from 25 to 90 °C, according to Grenthe et al.,[21] who reported a very small temperature dependency of the ion interaction coefficients between 25 and 200 °C (with $(\partial\varepsilon/\partial T)_p < 0.005$ $kg\cdot mol^{-1}\cdot K^{-1}$ at $T < 200$ °C). The obtained $\log_{10} {}^*\beta^\circ$ values at 40, 50, 60, 80, and 90 °C for $Cm(H_2PO_4)^{2+}$ and $Cm(H_2PO_4)_2^+$ are summarized in Tables 6 and 7. The uncertainties on $\log_{10} {}^*\beta^\circ(T)$ were obtained from the uncertainties on $\log_{10} {}^*\beta(T)$ and $\Delta\varepsilon$ as follows:

$$\sigma_{\log_{10}{}^*\beta^0} = \sqrt{\sigma^2_{\log_{10}{}^*\beta} + (m_{ClO_4^-}\cdot\sigma_{\Delta\varepsilon})^2} \quad (15)$$

Note that the conditional complexation constants at elevated temperatures taken from Jordan et al.[14] were extrapolated to infinite dilution using the ion interaction coefficients determined in the present study.

3.2.2.3. Derivation of Thermodynamic Functions. The standard molal enthalpy of reaction $\Delta_R H^0_m$ and standard molal entropy of reaction $\Delta_R S^0_m$ were obtained using the integrated van't Hoff equation (eq 16), assuming the $\Delta_R S^0_m$ value to remain constant between 25 and 90 °C. The same assumption was done for the molal enthalpy of reaction, assuming the molal standard heat capacity of reaction $\Delta_R C^0_{p,m}$ to be constant and equal to zero.

$$\log_{10} K^0(T) = \log_{10} K^0(T_0) + \frac{\Delta_r H^0(T_0)}{R\ln 10}\left(\frac{1}{T_0} - \frac{1}{T}\right) \quad (16)$$

with R being the universal molar gas constant (8.31451 $J\cdot K^{-1}\cdot mol^{-1}$) and T the temperature in Kelvin (T_0 = 298.15 K).

Results are shown in Figure 5, and explanations about the weighted least squares regression were already mentioned in Section 3.1.2.

The derived thermodynamic data are summarized in Table 8 together with the corresponding weighted sum of squared residuals (WSOSR). Covariance matrices are given in Table S1.

All thermodynamic functions for both complexes were found to be positive, meaning that the reactions were endothermic and entropy-driven. The temperature-dependent complexation constants were also described with the extended van't Hoff equation (see the Supporting Information). Interestingly, for the $Cm(H_2PO_4)^{2+}$ complex, considering the standard molal heat capacity of reaction does not significantly improve the WSOSR (1.612 vs 1.327) of the fit and delivers a $\Delta_R C^0_{p,m}$ value with a large uncertainty (cf. Table S2). The situation for the $Cm(H_2PO_4)_2^+$ complex is different. There, the WSOSR of the fit is improved by almost 1 order of magnitude (0.499 vs 0.073), which allows a better description of the data. Covariance matrices obtained with the extended van't Hoff equation are given in Table S3.

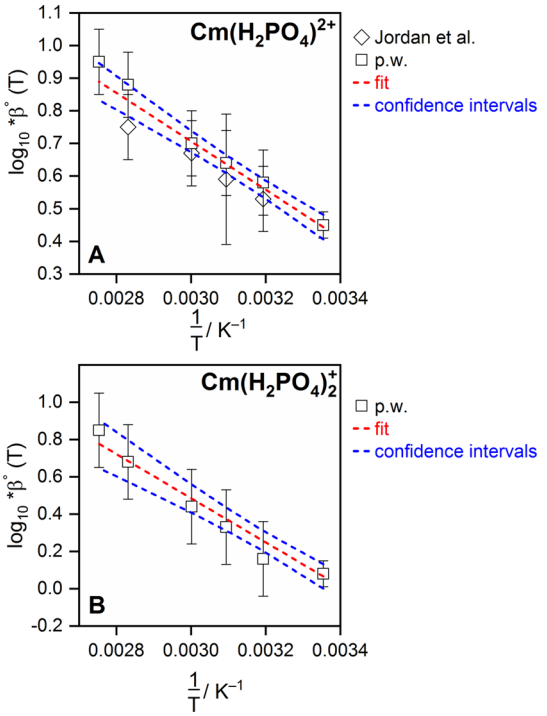

Figure 5. Van't Hoff plots for the $Cm(H_2PO_4)^{2+}$ (A) and $Cm(H_2PO_4)_2^+$ (B) complexes, based on the data in Tables 6 and 7.

Table 8. Thermodynamic Functions Derived for the $Cm(H_2PO_4)^{2+}$ and $Cm(H_2PO_4)_2^+$ Complexes Using the Integrated van't Hoff Equation

thermodynamic data	$Cm^{3+} + H_3PO_4 \rightleftharpoons Cm(H_2PO_4)^{2+} + H^+$	$Cm^{3+} + 2H_3PO_4 \rightleftharpoons Cm(H_2PO_4)_2^+ + 2H^+$
$\Delta_R H^0_m$ ($kJ\cdot mol^{-1}$)	14.2 ± 1.1	22.7 ± 1.8
$\Delta_R S^0_m$ ($J\cdot mol^{-1}\cdot K^{-1}$)	56.1 ± 3.3	77.3 ± 5.7
WSOSR	1.612	0.499

3.3. Cm(III) Complex Structures and Coordination.

3.3.1. Ab Initio Calculations. All the Cm(III) complexes with one or two dihydrogen phosphate ligands are found to host $H_2PO_4^-$ as a monodentate ligand in the solvated phase. Indeed, the Gibbs free energy of $[Cm(H_2O)_8H_2PO_4]^{2+}$ with exclusive monodentate bonds between the $H_2PO_4^-$ ligand and the curium is energetically lower by 10 $kJ\cdot mol^{-1}$ than the one for which the $H_2PO_4^-$ ligand is bidentately bound, a tendency that is reversed in the gas phase. The considered monodentate complexes are presented in Figure 6.

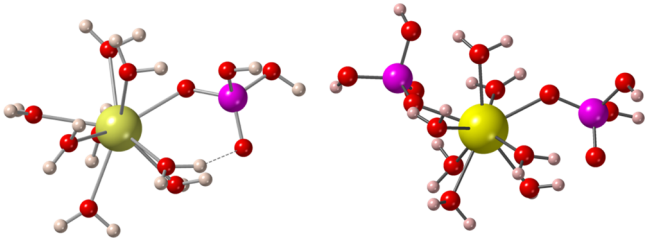

Figure 6. Complexes of $[Cm(H_2O)_8H_2PO_4]^{2+}$ (left) and $[Cm(H_2O)_7(H_2PO_4)_2]^+$ (right) optimized at the UMP2 level of theory (Cm are in yellow, O in red, H in white, P in violet). Dashed line = hydrogen bond.

https://doi.org/10.1021/acs.inorgchem.1c01319
Inorg. Chem. 2021, 60, 10656−10673

In the 1:1 complexes, the monodentate dihydrogen phosphate binds Cm at very short distances of 2.260 and 2.297 Å for the 8- and 9-coordinated complexes, respectively, while all Cm−OH_2 distances, except for a long one at 2.57 Å, lie between 2.44 and 2.53 Å, i.e., in the range of those computed for the Cm aqua ion (Table S4). For the 1:2 complexes, the distances to the monodendate oxygen atoms of the two dihydrogen phosphate groups appear to be longer by 0.05 Å for CN = 8 and 0.07 Å for CN = 9 than in the 1:1: complexes because of their mutual steric repulsion (Table S4). The very short distance between Cm and the interacting oxygen of the dihydrogen phosphate group plus the anionic character of the ligand may suggest that the character of this bond is different from that between Cm and a neutral water molecule. However, as observed in Table S5, the QTAIM analysis that compares the $Cm(H_2PO_4)^{2+}$ complex to the aqua complex shows that the Cm − $O_{H_2PO_4}$ bond is about the same type as the typical Cm − O_{H_2O} bond, which is essentially ionic, similar to other *An* or *Ln* ions interacting with inorganic or organic ligands.[58−60]

The exploration of the relative stability of hydrated species is also possible owing to the estimation of the Gibbs free energy of reactions $\Delta G_r(T)$, as defined in Section 2.4.3. Before discussing the computed QM numbers, one has to be aware that the accuracy of $\Delta G_r(T)$ QM calculations might be impacted by the COSMO solvation energies of charged species that can deviate by up to 30 kJ·mol^{-1} in absolute terms.[61] These errors are expected to largely compensate when considering reaction quantities. For reaction R1 involving exclusively the aqua ion, ΔG_r = +6 kJ·mol^{-1} at 25 °C and +0.7 kJ·mol^{-1} at 90 °C were computed, i.e., a constant number of coordination of nine is favored at 25 °C (about 90%). Albeit at 90 °C the population of 8-coordinated aqua ion increases, the coordination is still dominated by the 9-coordinated one. This result is fully consistent with the Gibbs free energy value ΔG_r = +5.5 kJ·mol^{-1}, estimated by Lindqvist-Reis et al.[62] For the 1:1 complexes, the computed Gibbs free energy of reaction for the reaction R2 corresponding to the water dissociation process from the 9-coordinated $[Cm(H_2O)_8(H_2PO_4)]^{2+}$ is endergonic, ΔG_r = +2.3 kJ·mol^{-1}, suggesting that the solution might contain a large amount of 9-coordinated species. For the 1:2 complexes, the ΔG_r associated with reaction R3 is estimated to be at −7.5 kJ·mol^{-1} at 25 °C, meaning that one would possibly expect a decrease of the coordination number from 9 to 8, a tendency reinforced by the rise of the temperature (ΔG_r = −13.9 kJ·mol^{-1} at 90 °C).

Based on the optimized Cm(III)−complex structures, the *ab initio* absorption/emission wavelengths of five considered $[Cm(H_2O)_n(H_2PO_4)_m]^{(3-m)+}$ complexes are reported, with $n + m = 8$ or 9 and n varying from 6 to 9. The data are available in Table S6 for a coordination number equal to 9 and Table S7 for CN = 8. They are associated with absorption energies averaged over the 8 spin−orbit components of the spin-free octet ground state to the lowest components of the sextet states. The absolute absorption energies are corrected by an estimated shift $\Delta E_{XMS\text{-}CASPT2}$ (as defined in Section 2.4.2).

For the $[Cm(H_2O)_9]^{3+}$ complex, geometry optimizations at the CASSCF level for the octet ground state and the lowest sextet state were carried out and it turned out that the changes in the Cm−OH_2 distances did not exceed a few picometers. This leads to the conclusion that one can compute emission energies and wavelengths using the ground-state octet geometry. Note that the resulting absolute absorption/emission energies might be slightly shifted with respect to experimental data as the chemical model and the method used to optimize the geometries might impact them; computed first-shell distances might be about 0.50 Å too long.[60,63] However, as shown in recent computational studies of Ce(III) spectroscopy,[60,64] one can expect the computed quantities to be accurate enough to discuss trends in emission energies with respect to changes in either the coordination number or the first-coordination shell ligand.

According to the quantum chemical calculations, the complexation of Cm with one or two hydrogen phosphate groups results in a small lowering of the emission energies by only a few hundreds cm^{-1} compared to the aqua ion, thus corresponding to a small red shift. This theoretical result is perfectly in line with the experimental observations (see Section 3.1.1) as well as our former study,[14] even though the computed redshift is slightly overestimated, as expected regarding the "computational" constraints.

For the sake of comparison with luminescence spectroscopic data acquisition, an additional and interesting feature that can be deduced from the simulations is the crystal field splitting (CFS) of the low-lying excited states of the complexes. Here, we specifically mean the few lowest components of the sextet states that are within 1000 cm^{-1} of the lowest one. In the 1:1 complex for CN = 9, the computed splitting $\Delta E(A_4 - A_1)$ of 432 cm^{-1} is slightly larger than the one in the 1:2 complex, i.e., 378 cm^{-1}, both being larger than what was found for the $[Cm(H_2O)_9]^{3+}$ aqua ion, i.e., 273 cm^{-1} (Table S6). Note that the reduction of the first-coordination sphere by one water molecule results in an increase of the crystal field splitting by a factor of 1.3 for the aqua ion and 1:1 complex and a factor of 1.5 for the 1:2 complex (see Tables S6 and S7, ratio $\Delta E(B_4 - B_1)/\Delta E(A_4 - A_1)$).

3.3.2. Luminescence Spectroscopy. In order to assess the complex structures in more detail and to account for potential changes in the overall coordination number with increasing temperature, the spectroscopic data in terms of obtained pure component spectra can be compared with the computed data for the Cm(III) electronic levels in the different complex coordinations (8-fold vs 9-fold).

From the obtained pure component spectra, the CFS can be determined when the emission profiles are fitted with four Lorentzian functions. The prerequisite for the fitting is that the population of these crystal field states follows the Boltzmann distribution (eq 3). The obtained peak positions of the four Lorentzian peaks can thereafter be compared to the computed crystal field splitting for the two identified Cm−phosphate complexes with an overall coordination number of 8 or 9.

For such comparison, one has to begin the discussion with the noncomplexed Cm^{3+} aqua ion. At 25 °C, more than 90% of the aqua ions have been shown to exist in solution as nine-hydrated tricapped-trigonal-prismatic $Cm(H_2O)_9^{3+}$ cations.[62] The remaining ∼10% are 8-fold coordinated $Cm(H_2O)_8^{3+}$ with a square-antiprismatic structure. With increasing temperature, the amount of 8-fold coordinated Cm^{3+} ions increases, so that at 90 °C (the highest temperature used in the present study) approximately 20% of the Cm^{3+} aqua ions have 8-fold coordination. The presence of both 8-fold and 9-fold coordinated Cm(III) can be directly observed in the measured Cm(III) aqua ion emission spectrum as a shoulder on the red side of the emission peak (see Figure S9). The emission spectrum collected at 90 °C has been fitted with two

https://doi.org/10.1021/acs.inorgchem.1c01319
Inorg. Chem. 2021, 60, 10656−10673

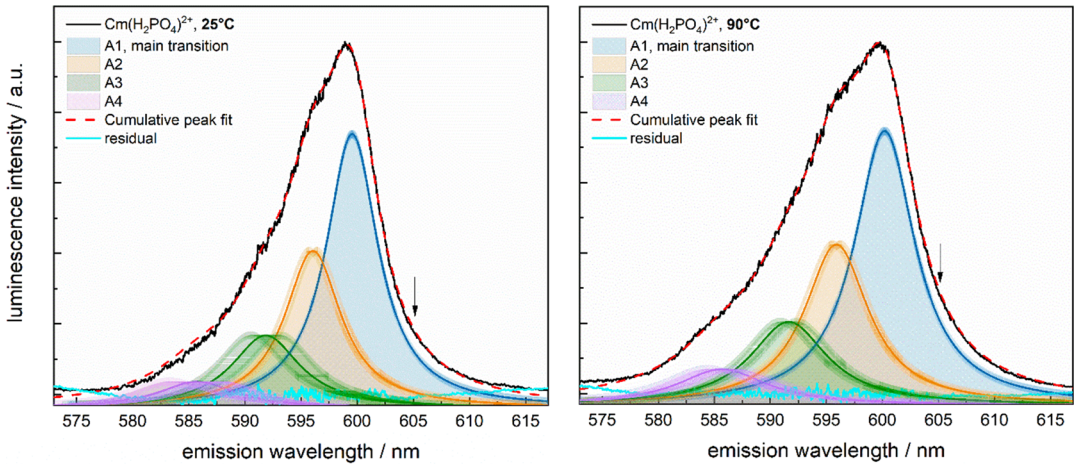

Figure 7. Extracted pure component emission spectra (black curves) of the $Cm(H_2PO_4)^{2+}$ complex at 25 (left) and 90 °C (right) can be described with four Lorentzian peaks following the Boltzmann distribution depicting the emission transitions from the four crystal field states of the excited electronic level (A_1−A_4) back to the ground state. Errors expressed with 99.7% (3σ) confidence of the fitted Lorentzian peak maxima and the fit residual (cyan traces) are included in the plots. Arrows indicate the part of the spectrum where the presence of an 8-fold coordinated $Cm(H_2PO_4)^{2+}$ complex would be expected to appear.

Table 9. Crystal Field Splitting (CFS) Obtained from the Fitted Experimental Pure Component Emission Spectra for the $Cm(H_2PO_4)^{2+}$ and $Cm(H_2PO_4)_2^{+}$ Complexes Are Compared with the Computed CFS for These Complexes in 8-Fold and 9-Fold Coordination

transition	exp. CFS 25 °C	exp. CFS 90 °C	comp. CFS CN = 9	ΔCFS 25 °C (comp.−exp.) CN = 9	ΔCFS 90 °C (comp.−exp.) CN = 9	comp. CFS CN = 8	ΔCFS 25 °C (comp.−exp.) CN = 8	ΔCFS 90 °C (comp.−exp.) CN = 8
				crystal field splitting of the 1:1 $Cm(H_2PO_4)^{2+}$ complex				
A_1	0	0	0	0	0	0	0	0
A_2	98 ± 9	117 ± 7	112	14	−5	165	67	48
A_3	217 ± 36	233 ± 19	291	74	58	303	86	70
A_4	364 ± 70	396 ± 35	432	68	36	565	201	169
				crystal field splitting of the 1:2 $Cm(H_2PO_4)_2^{+}$ complex				
A_1	0	0	0	0	0	0	0	0
A_2	170 ± 24	162 ± 6	128	−42	−34	141	−29	−21
A_3	301 ± 68	262 ± 21	229	−72	−33	241	−60	−21
A_4	451 ± 63	437 ± 54	378	−73	−59	573	122	136

approaches: (i) considering both coordinations of the aqua complex by fitting the main transitions (A_1) of both $Cm(H_2O)_9^{3+}$ and $Cm(H_2O)_8^{3+}$ and three composite hot-band transitions describing the 6 crystal field states (A_2−A_4) of the two aqua ion configurations and (ii) only considering the presence of 9-fold coordinated aqua ion with an overall of four crystal field transitions. The latter fit is clearly unsatisfactory, highlighting the visible presence of a significant amount of $Cm(H_2O)_8^{3+}$ in the measured emission spectrum collected at this elevated temperature. Further discussion of the obtained fit and resulting crystal field splitting in comparison to the computed one is given in the Supporting Information (see text and Table S8).

To explore the possibility of a change in coordination for the two extracted Cm(III)−phosphate complexes with increasing temperature, the extracted pure component spectra were analyzed in detail. We begin the discussion with the 1:1 $Cm(H_2PO_4)^{2+}$ complex. The extracted pure component emission spectra for this Cm−phosphate complex at 25 and 90 °C were fitted with four Lorentzian peaks (emission transition from the crystal field levels A_1−A_4 back to the ground state) following the Boltzmann distribution. This fit assumes that only one complex configuration (*e.g.*, only 8-fold or only 9-fold coordination) is present in solution at both temperatures. As illustrated in Figure 7, this fit reproduced the experimental data very well. No deviation on the red side of the spectrum (indicated in Figure 7 with an arrow), which would point toward the presence of an additional complex configuration as observed for the Cm(III) aqua ion, can be observed. The largest deviation from the extracted pure component emission spectrum can be seen at 25 °C around 585 nm, which can be related to the rather large error of the fitted peak position of the crystal field transition A_4 (errors for the Lorentzian peak centers are included in the plots in Figure 7). With increasing temperature, the population of the crystal field levels increases and the error associated with the Lorentzian fits of these hot-band transitions decreases. All fitted parameters with associated errors are compiled in Table S9.

At 90 °C, for the composite spectrum, the fitted Lorentzian functions of the $Cm(H_2PO_4)^{2+}$ complex are broader than at 25 °C, owing to inhomogeneous broadening of the spectral lines with increasing temperature.[65] From the obtained peak maxima of the Lorentzian peaks, representative of the energy of the crystal field transitions, the magnitude of the crystal field splitting can be calculated. The results are compiled in Table 9 together with the computed crystal field splitting for the Cm(III)−phosphate complex in 8-fold and 9-fold coordina-

https://doi.org/10.1021/acs.inorgchem.1c01319
Inorg. Chem. 2021, 60, 10656−10673

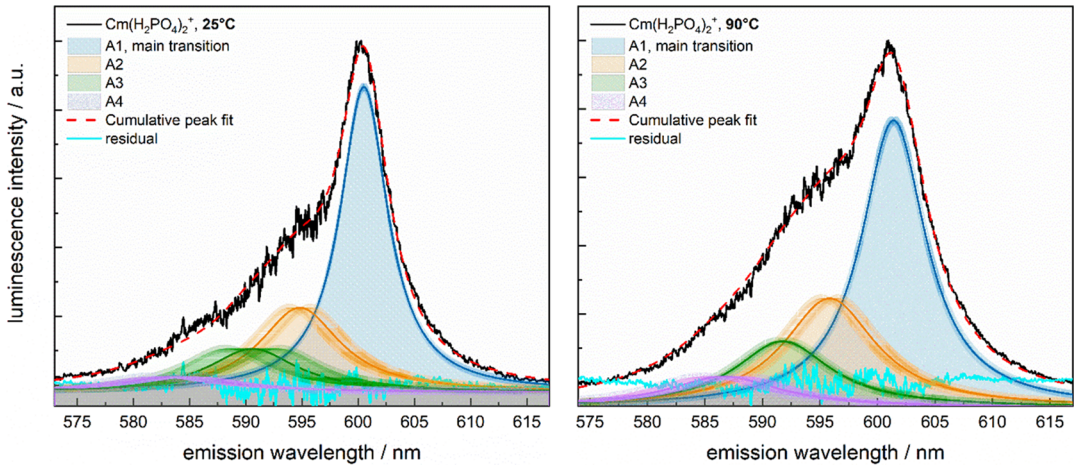

Figure 8. Extracted pure component emission spectra (black curves) of the $Cm(H_2PO_4)_2^+$ complex at 25 (left) and 90 °C (right) can be described with four Lorentzian peaks following the Boltzmann distribution depicting the emission transitions from the four crystal field states of the excited electronic level (A_1–A_4) back to the ground state. Errors expressed with 99.7% (3σ) confidence of the fitted Lorentzian peak maxima and the fit residual (cyan traces) are included in the plots.

tion. The magnitude of the crystal field splitting at the two investigated temperatures is very similar, yielding average values of 0 (A_1), 107 (A_2–A_1), 224 (A_3–A_1), and 380 (A_4–A_1). This splitting is in excellent agreement with the computed crystal field splitting for the $Cm(H_2PO_4)^{2+}$ complex with an overall coordination number of 9 (see Table 9). Therefore, this Cm(III)–phosphate complex can with confidence be assigned to the 9-fold coordinated $Cm(H_2O)_8(H_2PO_4)^{2+}$ species. Based on the identical crystal field splitting at 25 and 90 °C and the absence of any features in the extracted pure component emission spectra, which cannot be described using the four Lorentzian peaks, this coordination is preserved over the entire investigated temperature range. In other words, a similar decrease of the coordination number from 9 to 8 as observed for the curium aqua ion as a function of temperature does not occur for this phosphate complex.

A similar treatment of the pure component spectra for the $Cm(H_2PO_4)_2^+$ complex was done to obtain the crystal field splitting at 25 and 90 °C. The obtained results for these two temperatures are shown in Figure 8. The experimental and computational data of the crystal field splitting are compiled in Table 9, while a summary of all fitting parameters can be found in Table S10.

In contrast to the 1:1 species where the computed crystal field splitting for the 8-fold and 9-fold coordinated $Cm(H_2PO_4)^{2+}$ complex is clearly different, a very similar splitting is obtained for both coordinations of the $Cm(H_2PO_4)_2^+$ complex (see Table 9). The largest difference can be seen for the A_4–A_1 band gap, which unfortunately inherits the largest error in the fitted experimental profiles due to the low population of the highest crystal field level, especially at 25 °C. When omitting this level from the comparison, a better fit with the computed data for the 8-fold coordinated complex can be deduced. If the A_4 level is included, the 9-fold coordinated species seems to yield the most consistent result, which is in agreement with the coordination of the 1:1 complex. Therefore, a direct conclusion of the coordination of this species is hard to draw.

In comparison to the fitted profiles of the 1:1 complex, the fitting residual of the 1:2 complex (cyan traces in Figure 8) is larger. The worse fit of the latter complex is also visible from the SOSR values (compiled for all fits in Table S11), which is larger by a factor of 2 at 25 °C and by a factor of almost 4 at 90 °C in comparison to the values obtained for the 1:1 complex. As our computational results point toward a possible presence of 8-fold coordinated $Cm(H_2PO_4)_2^+$, the fit was redone with addition of a fifth Lorentzian function describing the A_1 transition of such an 8-fold coordinated complex configuration (similar to the procedure described above for the aqua ion). To facilitate the interpretation of the results, pure component spectra for the 1:2 complex collected at 40, 60, and 80 °C were included in the data treatment. The results for all five temperatures are compiled in Figure S10 and Table S12. At 25 and 40 °C, the fits are not improved by the inclusion of this fifth Lorentzian component depicting the presence of $Cm(H_2PO_4)_2^+$ with CN = 8 (see Table S11). At 60–90 °C, however, the SOSR become systematically better with five components rather than four, which serves as an indication for the presence of 8-fold coordinated $Cm(H_2O)_6(H_2PO_4)_2^+$ in addition to $Cm(H_2O)_7(H_2PO_4)_2^+$ in 9-fold coordination. Based on the area under the curves of the main transition (A_1) peaks, the amount of 8-fold coordinated species increases from 2% at 25 °C to 14% at 90 °C. However, as the individual hot-band transitions of both coordinations cannot be resolved and hot-bands of the 8-fold coordinated complex can be expected to overlap with the main transition of the 9-fold coordinated species, these values should be taken as tentative, yielding information of the trends in the system rather than the absolute speciation.

4. DISCUSSION

Based on our luminescence spectroscopic data, three different Cm(III)–phosphate complexes could be derived from our peak deconvolution. Only two complexes could be identified in solution at the lower investigated pH value of $-\log_{10}[H^+]$ = 2.52. Based on slope analysis of the derived species distributions, these two species could be assigned to $Cm(H_2PO_4)^{2+}$ and $Cm(H_2PO_4)_2^+$ with complexation constants at infinite dilution of $\log_{10} {}^*\beta^0 = 0.45 \pm 0.04$ (reaction R4) and $\log_{10} {}^*\beta^0 = 0.08 \pm 0.07$ (reaction R5), respectively. Recalculating these values for the reactions $Cm^{3+} + H_2PO_4^- \rightleftharpoons Cm(H_2PO_4)^{2+}$ and $Cm^{3+} + 2\ H_2PO_4^- \rightleftharpoons Cm(H_2PO_4)_2^+$ using the reaction $H^+ + H_2PO_4^- \rightleftharpoons H_3PO_4$ ($\log_{10} \beta^\circ = 2.14 \pm$

https://doi.org/10.1021/acs.inorgchem.1c01319
Inorg. Chem. 2021, 60, 10656–10673

0.03)[21] yields complexation constants of $\log_{10}\beta^0 = 2.59 \pm 0.05$ and $\log_{10}\beta^0 = 4.36 \pm 0.09$. The complexation constant for the 1:1 complex is identical to the one derived in our previous study (2.59 ± 0.19);[14] however, due to the larger amount of data points used for the extrapolation and recalculation of the complexation constant and the slightly different statistical approach in the present work, the uncertainty is substantially smaller. This is the first time that a complex stoichiometry of 1:2 for the second Cm(III)−phosphate complex is spectroscopically confirmed and that consistent thermodynamic data are provided since the two most recent studies compiled in Table 1, accounting for more than one *An*−phosphate complex, only report $An(H_2PO_4)^{2+}$ and $An(HPO_4)^{+}$ species (*An* = Am or Cm).[15,18] In both the studies of Moskvin[17] and Lebedev et al.,[20] however, the formation of 1:2 $An(H_2PO_4)_2^{+}$ complexes has been proposed. In the latter study, slope analysis of the spectrophotometric data yielded a complexation constant of 3.72 ± 0.02 for $Am(H_2PO_4)_2^{+}$, a value that is substantially lower than the corresponding one for the $Cm(H_2PO_4)_2^{+}$ complex reported in the present study. Lebedev et al.,[20] however, worked at very high total phosphate concentrations (up to 13 mol·L^{-1}), and the ionic strength was not kept constant in their study. Therefore, this complex and the postulated complexation constant were not accepted by Silva et al.[22] with the explanation that the experimental conditions in terms of the very high ionic strength could lead to ionic strength artifacts such as the decrease of the molar extinction coefficient in the quasi "nonaqueous" media. Thus, our study is the first one to report a complexation constant for the 1:2 complex under controlled ionic strength conditions.

The interaction coefficient $\varepsilon(Cm(H_2PO_4)^{2+};ClO_4^{-})$ (0.17 ± 0.04 kg·mol^{-1}) was found to be larger than $\varepsilon(Cm(H_2PO_4)_2^{+};ClO_4^{-})$ (−0.10 ± 0.06 kg·mol^{-1}), which can be attributed to the higher charge density of the $Cm(H_2PO_4)^{2+}$ complex. This is in line with the computed bond length between Cm and the oxygen atoms of the dihydrogen phosphate ligand, which is shorter in the $Cm(H_2PO_4)^{2+}$ complex (see Section 3.3.1).

As the temperature increases from 25 to 90 °C, the relative permittivity of water, or more commonly called dielectric constant ε_r, decreases from 78 to 58, due to an increased thermal agitation in the system, leading to an increased entropy coming from an increased disorder. This, combined with the release of one or two H_2O molecules from the first coordination shell of the aqua ion upon complexation of the $H_2PO_4^{-}$ ligand(s), contributes to the overall increase in entropy, in agreement with the positive $\Delta_R S_m^0$ values derived from the application of the integrated van't Hoff equation to the temperature-dependent data.

Based on our *ab initio* calculations, both the 1:1 and 1:2 Cm−phosphate complexes with monodentate coordination to the $H_2PO_4^{-}$ ligand are the most stable complex configurations at 25 °C. This coordination is supported by our luminescence lifetime measurements, where a very small increase of the overall luminescence lifetime was observed with increasing phosphate complexation. As previously mentioned, the lifetimes could be well described by the coordination of 8 or 7 H_2O entities to the curium cation in the $Cm(H_2PO_4)^{2+}$ and $Cm(H_2PO_4)_2^{+}$ complexes, respectively, using (eq 4), proposed by Kimura and Choppin.[55] When preserving an overall Cm(III) coordination number of 9, only monodentate coordination to the $H_2PO_4^{-}$ ligand is possible.

At elevated temperature, however, our *ab initio* simulations predict a different behavior in terms of the coordination, for the two identified Cm(III)−phosphate complexes. For the $Cm(H_2PO_4)^{2+}$ species, the coordination number is predominantly 9 both at 25 and 90 °C, which is in agreement with the deconvolution and subsequent Boltzmann fitting of the luminescence emission spectra (see Section 3.3.2). However, for the $Cm(H_2PO_4)_2^{+}$ complex, a decrease of the coordination number from 9 to 8 could be favored. Indeed, in this stoichiometry, the two hydrogens of the phosphate groups sterically repel each other, inducing a lengthening of some Cm−OH_2O bond lengths, thus making the water molecules more labile. Note that the presence of the $Cm(H_2PO_4)_2^{+}$ complex with both coordination number of 8 and 9 leads to an increased disorder. In addition, both *ab initio* simulations (see Section 3.3.1) and deconvolution of the luminescence spectra (see Section 3.3.2) revealed an increased amount of 8-fold coordinated Cm^{3+} ions with temperature (≈14% at 90 °C). The decrease of the coordination number of the Cm(III) aqua ion as a function of temperature was found to be entropy-driven (ΔS = 25.4 ± 1.2 J·mol^{-1}·K^{-1}).[62] This could also be a driving force to the decreased coordination number for the 1:2 $Cm(H_2PO_4)_2^{+}$ complex.

The unfavorable enthalpy of reaction observed for both Cm−phosphate complexes reveals that the heat spent in the loss of water molecules is not regained upon interaction of the $H_2PO_4^{-}$ ligand(s) with the Cm^{3+} ion. Interestingly, the temperature-dependent complexation data of the $Cm(H_2PO_4)^{2+}$ complex is well described using the integrated van't Hoff equation. For the $Cm(H_2PO_4)_2^{+}$ complex, the fit was improved by 1 order of magnitude when the extended van't Hoff equation was applied. Both integrated and extended van't Hoff equations possess two fit parameters; therefore, the decreased WSOSR for the extended van't Hoff equation is not due to the presence of a different number of variables to be fitted.

This could be the result of the presence of two $Cm(H_2O)_7(H_2PO_4)_2^{+}$ and $Cm(H_2O)_6(H_2PO_4)_2^{+}$ species being 9-fold and 8-fold coordinated, respectively, with temperature-dependent fractions (see Section 3.3.2). This would imply that the "single pure" component spectrum derived from the luminescence data for the 1:2 complex would in fact correspond to a mixture of 8-fold and 9-fold coordinated species. The same is true for the Cm^{3+} aqua ion (see Section 3.3.2). Ideally, one should extract the relative distribution of Cm^{3+} and $Cm(H_2PO_4)_2^{+}$ with CN = 8 and CN = 9 during the deconvolution of the luminescence spectra. However, this is not possible as the increase of temperature does not only lead to an increase of the 8-fold coordinated species but also to an increase of the hot-band intensities of both the 9-fold and 8-fold coordinated species. Therefore, a difference spectrum aiming at extracting the emission spectrum of $Cm(H_2O)_6^{+}(H_2PO_4)_2$ would show additional peaks belonging to the hot-band transitions of the $Cm(H_2O)_7^{+}(H_2PO_4)_2$ complex. With individual components, it would be conceivable to apply the SIT theory for two species with different coordination numbers if their relative proportion is known and to derive for each of them a complexation constant at infinite dilution together with an ion interaction coefficient. Subsequently, the integrated van't Hoff equation could be applied to obtain enthalpies and entropies of reaction for the 8- and 9-fold coordinated species. Eventually, the derived complexation constants at infinite dilution taking into account changes in the

https://doi.org/10.1021/acs.inorgchem.1c01319
Inorg. Chem. 2021, 60, 10656−10673

coordination number could be implemented in thermodynamic databases, by including the water molecules in the first hydration shell of the ions/complexes. Common geochemical speciation software can already handle water molecules in chemical reactions in which they get deprotonated (e.g., hydrolysis reactions) or for solubility products of solid phases containing water of hydration. Including the water molecules in the first hydration shell of ions/complexes is currently not possible and would require further code developments.

The decrease of the coordination number upon increasing temperature could not only apply to the Cm−phosphate system but as well to complexation studies with other inorganic ligands such as nitrate, sulfate, hydroxide, etc. This phenomenon is unfortunately simply overlooked in almost all complexation studies. Our results indicate that this aspect should be systematically examined, in particular when it comes to chemical species with more than one ligand in their first coordination sphere, which was shown to favor a decrease in the coordination number for the Cm(III)−phosphate system at elevated temperatures. Nevertheless, the authors are fully aware that this suggestion represents a significant amount of work, and if undertaken, it should be at first performed for species to be found under the geochemical conditions (E_h, pH, I, etc.) of nuclear waste repositories. Furthermore, greater uncertainties on the status of the repository, on conceptual and mathematical models, and on data and parameters will certainly exist.

When increasing the pH to $-\log_{10}[H^+] = 3.44-3.65$, the presence of a third Cm(III)−phosphate complex could be observed in the current study. Due to the overall low amount of this species, however, a reliable slope analysis could not be performed and we can only tentatively assign this species to the $Cm(HPO_4)^+$ complex identified in the studies by Rao et al.[18] and Moll et al.[15] At the chosen solution conditions in the present work, we are very close to the solubility limit of solid $CmPO_4{\cdot}xH_2O$ based on existing solubility data for amorphous $AmPO_4{\cdot}xH_2O$[25] and crystalline $LnPO_4{\cdot}0.667H_2O$ rhabdophane.[24] Therefore, finding suitable solution conditions where an adequate amount of $Cm(HPO_4)^+$ complex is present in solution while avoiding Cm−phosphate precipitation will be challenging even with such a sensitive spectroscopic method as luminescence spectroscopy allowing for the detection of subnanomolar Cm(III) concentrations. Alternatively, solid $CmPO_4{\cdot}xH_2O$ could be deliberately precipitated from solution and characterized with luminescence spectroscopy in order to determine a luminescence emission spectrum for this colloidal species. This would allow for analysis of suspensions where both such a precipitate and aqueous Cm(III)−phosphate species coexist in solution. This will require careful planning of the experiments as the amount of aqueous Cm(III) must be determined reliably to allow for the subsequent thermodynamic calculations, which requires a separation method such as ultracentrifugation, capable of removing nanoparticulate matter without introducing foreign substances into the system, i.e., from nanoporous filter materials. Thus, the further exploration of aqueous Cm(III)−phosphate species such as the formation of 1:1 and/or 1:2 $Cm(HPO_4)^+$ and $Cm(HPO_4)_2^-$ complexes must be the scope of well-designed future studies to be able to assess the relevance of aqueous *An*(III)-phosphate species in circumneutral and slightly alkaline (ground)waters.

5. CONCLUSIONS

In this study, we investigated the complexation of Cm(III) with aqueous phosphates using luminescence spectroscopy as the speciation tool. Three complexes could be identified in the phosphate-containing solutions, namely, $Cm(H_2PO_4)^{2+}$, $Cm(H_2PO_4)_2^+$, and presumably $Cm(HPO_4)^+$. For the former two complexes, present in sufficient abundance, conditional complexation constants at several ionic strengths (0.5−3.0 mol·L^{-1} $NaClO_4$) could be derived, which were extrapolated to standard conditions using the specific ion interaction theory (SIT). This way, ion interaction coefficients $\varepsilon(Cm(H_2PO_4)_n^{(3-n)+};ClO_4^-)$ (n = 1, 2) for the charged Cm(III)−phosphate species interacting with the electrolyte anions could be obtained. Temperature-dependent complexation constants were derived from luminescence data collected in the temperature range of 25−90 °C. By applying the integrated and extended van't Hoff equations, the molal enthalpy $\Delta_R H_m^0$ and molal entropy $\Delta_R S_m^0$ of reaction for the two Cm(III)−phosphate complexes could be derived. For the $Cm(H_2PO_4)^{2+}$ species, the temperature-dependent data was well described with the former equation, while a better fit was obtained for $Cm(H_2PO_4)_2^+$, when including the standard molal heat capacity of reaction. The underlying reason for this different temperature-dependent behavior could be a slightly different coordination chemistry of these complexes. By combining *ab initio* calculations with a thorough analysis of the obtained luminescence spectroscopic data, we could show that both $Cm(H_2PO_4)^{2+}$ and $Cm(H_2PO_4)_2^+$ complexes with an overall CN of 9 are stable in solution at 25 °C. This coordination is preserved for the former complex in the investigated temperature range up to 90 °C. For the latter complex, an increasing amount of 8-fold coordinated species could be established with increasing temperature. Such a coordination change may be of relevance for the complexation of f-elements with several other inorganic and/or organic systems, which to date have only been described with one overall complex configuration. With the development of new computational tools and sensitive spectroscopic methods, the possibility for derivation of individual thermodynamic data for complexes in different coordination, to accurately describe the speciation of inorganic and organic complexes and their temperature-dependent behavior in aqueous systems, should be explored.

■ ASSOCIATED CONTENT

Supporting Information

The Supporting Information is available free of charge at https://pubs.acs.org/doi/10.1021/acs.inorgchem.1c01319.

Atomic coordinates (ZIP)

All experimental data allowing derivation of the conditional complexation constants (XLSX)

Cm(III) species distribution at different ionic strengths and temperatures, Cm(III) emission spectra and luminescence lifetime fits, slope analysis for the Cm(III)-phosphate complexes, statistical description of the extended van't Hoff equation and derivation of thermodynamic functions, $Cm-OH_2$, $Cm-O_P$, and $Cm-P_P$ distances for the Cm(III) aqua ions and Cm(III)−phosphate complexes with coordination number 8 or 9 as well as their charges from ab initio simulations, computed absorption energies and crystal field splitting (CFS) of the Cm(III) aqua ion and the

https://doi.org/10.1021/acs.inorgchem.1c01319
Inorg. Chem. 2021, 60, 10656−10673

Cm(III)-phosphate complexes, description of the fitting of the luminescence data (PDF)

AUTHOR INFORMATION

Corresponding Authors

Florent Réal − *Univ. Lille, CNRS, UMR 8523 - PhLAM - Physique des Lasers Atomes et Molécules, F-59000 Lille, France*; orcid.org/0000-0002-5163-1545; Phone: +33 3 2033 5929; Email: florent.real@univ-lille.fr

Norbert Jordan − *Institute of Resource Ecology, Helmholtz - Zentrum Dresden - Rossendorf, Dresden 01328, Germany*; orcid.org/0000-0002-4625-1580; Phone: +49 351 260 2148; Email: n.jordan@hzdr.de

Authors

Nina Huittinen − *Institute of Resource Ecology, Helmholtz - Zentrum Dresden - Rossendorf, Dresden 01328, Germany*; orcid.org/0000-0002-9930-2329

Isabelle Jessat − *Institute of Resource Ecology, Helmholtz - Zentrum Dresden - Rossendorf, Dresden 01328, Germany*

Valérie Vallet − *Univ. Lille, CNRS, UMR 8523 - PhLAM - Physique des Lasers Atomes et Molécules, F-59000 Lille, France*; orcid.org/0000-0002-2202-3858

Sebastian Starke − *Computational Science Group (FWCC), Department of Information Services and Computing (FWC), Helmholtz - Zentrum Dresden - Rossendorf, 01328 Dresden, Germany*

Manuel Eibl − *Institute of Resource Ecology, Helmholtz - Zentrum Dresden - Rossendorf, Dresden 01328, Germany*

Complete contact information is available at: https://pubs.acs.org/10.1021/acs.inorgchem.1c01319

Notes

The authors declare no competing financial interest.

ACKNOWLEDGMENTS

This work was supported by the German Federal Ministry of Education and Research (BMBF), Project No. 02NUK039B (ThermAc) and 033R127D (SEM^2). F.R. and V.V. acknowledge support by the French government through the Program "Investissement d'avenir" (LABEX CaPPA/ANR−11−LABX−0005−01 and I−SITE ULNE/ANR−16−IDEX−0004 ULNE), by the Ministry of Higher Education and Research, Hauts de France Council and European Regional Development Fund (ERDF) through the Contrat de Projets État−RÉgion (CPER−CLIMIBIO), as well as by the French research network GDR 2035 SolvATE. Furthermore, this work was granted access to the HPC resources of [CINES/IDRIS/TGCC] under the allocation 2019−2020 [A0070801859] made by GENCI.

REFERENCES

(1) Runde, W. The Chemical Interactions of Actinides in the Environment. *Los Alamos Science* **2000**, *26*, 392−411.

(2) Silva, R. J.; Nitsche, H. Actinide Environmental Chemistry. *Radiochim. Acta* **1995**, *70-71*, 377−396.

(3) Maher, K.; Bargar, J. R.; Brown, G. E., Jr. Environmental Speciation of Actinides. *Inorg. Chem.* **2013**, *52*, 3510−3532.

(4) Nahas, E. Factors determining rock phosphate solubilization by microorganisms isolated from soil. *World J. Microbiol. Biotechnol.* **1996**, *12*, 567−572.

(5) Jones, D. L.; Oburger, E. In *Phosphorus in Action: Biological Processes in Soil Phosphorus Cycling*; Bünemann, E., Oberson, A., Frossard, E., Ed.; Springer Berlin Heidelberg: Berlin, Heidelberg, 2011; pp. 169−198.

(6) Holtan, H.; Kamp-Nielsen, L.; Stuanes, A. O. Phosphorus in soil, water and sediment: an overview. *Hydrobiologia* **1988**, *170*, 19−34.

(7) Sharpley, A. N.; Daniel, T. C.; Edwards, D. R. Phosphorus Movement in the Landscape. *J. Prod. Agric.* **1993**, *6*, 492−500.

(8) Sims, J. T.; Simard, R. R.; Joern, B. C. Phosphorous Loss in Agricultural Drainage: Historical Perspectives and Current Research. *J. Environ. Qual.* **1998**, *27*, 277−293.

(9) Yuan, Z.; Shi, J.; Wu, H.; Zhang, L.; Bi, J. Understanding the anthropogenic phosphorus pathway with substance flow analysis at the city level. *J. Environ. Manage.* **2011**, *92*, 2021−2028.

(10) Ewing, R. C.; Wang, L. Phosphates as nuclear waste forms. *Rev. Mineral. Geochem.* **2002**, *48*, 673−699.

(11) Oelkers, E. H.; Montel, J.-M. Phosphates and Nuclear Waste Storage. *Elements* **2008**, *4*, 113−116.

(12) Dacheux, N.; Clavier, N.; Podor, R. Versatile Monazite: Resolving geological records and solving challenges in materials science. Monazite as a promising long-term radioactive waste matrix: Benefits of high-structural flexibility and chemical durability. *Am. Mineral.* **2013**, *98*, 833−847.

(13) Huittinen, N.; Scheinost, A. C.; Ji, Y.; Kowalski, P. M.; Arinicheva, Y.; Wilden, A.; Neumeier, S.; Stumpf, T. A Spectroscopic and Computational Study of Cm^{3+} Incorporation in Lanthanide Phosphate Rhabdophane ($LnPO_4.0.67H_2O$) and Monazite ($LnPO_4$). *Inorg. Chem.* **2018**, *57*, 6252−6265.

(14) Jordan, N.; Demnitz, M.; Lösch, H.; Starke, S.; Brendler, V.; Huittinen, N. Complexation of Trivalent Lanthanides (Eu) and Actinides (Cm) with Aqueous Phosphates at Elevated Temperatures. *Inorg. Chem.* **2018**, *57*, 7015−7024.

(15) Moll, H.; Brendler, V.; Bernhard, G. Aqueous curium(III) phosphate species characterized by time-resolved laser-induced fluorescence spectroscopy. *Radiochim. Acta* **2011**, *99*, 775−782.

(16) Morgenstern, A. Humat-und Phosphatkomplexierung von Actinidionen im grundwasserrelevanten pH-Bereich. Ph.D. thesis, Technische Universität München, Garching, 1997.

(17) Moskvin, A. I. Complex formation of the actinides with anions of acids in aqueous solutions. *Sov. Radiochem.* **1969**, *11*, 447−449.

(18) Rao, V. K.; Mahajan, G. R.; Natarajan, P. R. Phosphate Complexation of Americium (III). *Radiochim. Acta* **1986**, *40*, 145−149.

(19) Borisov, M. S.; Elesin, A. A.; Lebedev, I. A.; Filimonov, V. T.; Yakovlev, G. N. Investigation of the complexing of trivalent actinides and lanthanides in phosphoric acid solutions. *Sov. Radiochem.* **1966**, *8*, 40−44.

(20) Lebedev, I. A.; Frenkel, V. Y.; Kulyako, Y. M.; Myasoedov, B. F. Investigation of complex formation of Americium(III) and Americium(IV) in phosphoric acid solutions. *Sov. Radiochem.* **1979**, *21*, 692−698.

(21) Grenthe, I.; Gaona, X.; Plyasunov, A. V.; Rao, L.; Runde, W. H.; Grambow, B.; Konings, R. J. M.; Smith, A. L.; Moore, E. M. *Second Update on the Chemical Thermodynamics of Uranium, Neptunium, Plutonium, Americium and Technetium*; OECD Publications: Paris, 2020.

(22) Silva, R. J.; Bidoglio, G.; Rand, M. H.; Robouch, P. B.; Wanner, H.; Puigdomenech, I. *Chemical Thermodynamics of Americium*; Elsevier: North-Holland, 1995.

(23) Moskvin, A. I. Investigation of the complex formation of trivalent plutonium, americium and curium in phosphate solutions. *Sov. Radiochem.* **1971**, *13*, 688−693.

(24) Gausse, C.; Szenknect, S.; Qin, D. W.; Mesbah, A.; Clavier, N.; Neumeier, S.; Bosbach, D.; Dacheux, N. Determination of the Solubility of Rhabdophanes $LnPO_4{\cdot}0.667H_2O$ (Ln = La to Dy). *Eur. J. Inorg. Chem.* **2016**, *2016*, 4615−4630.

(25) Rai, D.; Felmy, A. R.; Fulton, R. W. Solubility and Ion Activity of $AmPO_4{\cdot}xH_2O$. *Radiochim. Acta* **1992**, *56*, 7−14.

(26) Parkhurst, D. L.; Appelo, C. A. J. *Description of input and examples for PHREEQC version 3—A computer program for speciation, batch-reaction, one-dimensional transport, and inverse geochemical*

calculations; U.S. Geological Survey Techniques and Methods, book 6, chap. A43: 2013.
(27) Giffaut, E.; Grivé, M.; Blanc, P.; Vieillard, P.; Colàs, E.; Gailhanou, H.; Gaboreau, S.; Marty, N.; Madé, B.; Duro, L. Andra thermodynamic database for performance assessment: ThermoChimie. *Appl. Geochem.* **2014**, *49*, 225−236.
(28) Söhnel, O.; Novotný, P. *Densities of aqueous solutions of inorganic substances*; Elsevier: Amsterdam, 1985.
(29) *MATLAB 2019 (Version 2)*; Natick, Massachusetts, United States.
(30) *OriginPro, Version 2019*; OriginLab Corporation: Northampton, MA, USA.
(31) Huittinen, N.; Rabung, T.; Schnurr, A.; Hakanen, M.; Lehto, J.; Geckeis, H. New insight into Cm(III) interaction with kaolinite - Influence of mineral dissolution. *Geochim. Cosmochim. Acta* **2012**, *99*, 100−109.
(32) Eibl, M.; Virtanen, S.; Pischel, F.; Bok, F.; Lönnrot, S.; Shaw, S.; Huittinen, N. A spectroscopic study of trivalent cation (Cm^{3+} and Eu^{3+}) sorption on monoclinic zirconia (ZrO_2). *Appl. Surf. Sci.* **2019**, *487*, 1316−1328.
(33) Hättig, C.; Hellweg, A.; Köhn, A. Distributed memory parallel implementation of energies and gradients for second-order Møller−Plesset perturbation theory with the resolution-of-the-identity approximation. *Phys. Chem. Chem. Phys.* **2006**, *8*, 1159−1169.
(34) Hättig, C.; Weigend, F. CC2 excitation energy calculations on large molecules using the resolution of the identity approximation. *J. Chem. Phys.* **2000**, *113*, 5154−5161.
(35) Weigend, F.; Köhn, A.; Hättig, C. Efficient use of the correlation consistent basis sets in resolution of the identity MP2 calculations. *J. Chem. Phys.* **2002**, *116*, 3175−3183.
(36) Hättig, C. Optimization of auxiliary basis sets for RI-MP2 and RI-CC2 calculations: Core−valence and quintuple-ζ basis sets for H to Ar and QZVPP basis sets for Li to Kr. *Phys. Chem. Chem. Phys.* **2005**, *7*, 59−66.
(37) Cao, X.; Dolg, M. Segmented contraction scheme for small-core actinide pseudopotential basis sets. *J. Mol. Struct.: THEOCHEM* **2004**, *673*, 203−209.
(38) Weigend, F.; Häser, M.; Patzelt, H.; Ahlrichs, R. RI-MP2: optimized auxiliary basis sets and demonstration of efficiency. *Chem. Phys. Lett.* **1998**, *294*, 143−152.
(39) Frisch, M. J.; Trucks, G. W.; Schlegel, H. B.; Scuseria, G. E.; Robb, M. A.; Cheeseman, J. R.; Scalmani, G.; Barone, V.; Petersson, G. A.; Nakatsuji, H.; Li, X.; Caricto, M.; Marenich, A. V.; Bloino, J.; Janesko, B. G.; Gomperts, R.; Mennucci, B.; Hratchian, H. P.; Ortiz, J. V.; Izmaylov, A. F.; Sonnenberg, J. L.; Williams-Young, D.; Ding, F.; Lipparini, F.; Egidi, F.; Goings, J.; Peng, B.; Petrone, A.; Henderson, T.; Ranasinghe, D.; Zakrzewski, V. G.; Gao, J.; Rega, N.; Zheng, G.; Liang, W.; Hada, M.; Ehara, M.; Toyota, K.; Fukuda, R.; Hasegawa, J.; Ishida, M.; Nakajima, T.; Honda, Y.; Kitao, O.; Nakai, H.; Vreven, T.; Throssell, K.; Montgomery, J. A., Jr.; Peralta, J. E.; Ogliaro, F.; Bearpark, M. J.; Heyd, J. J.; Brothers, E. N.; Kudin, K. N.; Staroverov, V. N.; Keith, T. A.; Kobayashi, R.; Normand, J.; Raghavachari, K.; Rendell, A. P.; Burant, J. C.; Iyengar, S. S.; Tomasi, J.; Cossi, M.; Millam, J. M.; Klene, M.; Adamo, C.; Cammi, R.; Ochterski, J. W.; Martin, R. L.; Morokuma, K.; Farkas, O.; Foresman, J. B.; Fox, D. J. *Gaussian 16, Revision B.01*; Wallingford CT: 2016.
(40) Todd, A.; Keith, T. K. *AIMAll (Version 17.11.14)*; Gristmill Software: (aim.tkgristmill.com): Overland Park KS, USA, 2019.
(41) Klamt, A.; Schürmann, G. COSMO: A New Approach to Dielectric Screening in Solvents with Explicit Expressions for the Screening Energy and its Gradient. *J. Chem. Soc.-Perkin Trans. 2* **1993**, 799−805.
(42) Balasubramani, S. G.; Chen, G. P.; Coriani, S.; Diedenhofen, M.; Frank, M. S.; Franzke, Y. J.; Furche, F.; Grotjahn, R.; Harding, M. E.; Hattig, C.; Hellweg, A.; Helmich-Paris, B.; Holzer, C.; Huniar, U.; Kaupp, M.; Khah, A. M.; Khani, S. K.; Muller, T.; Mack, F.; Nguyen, B. D.; Parker, S. M.; Perlt, E.; Rappoport, D.; Reiter, K.; Roy, S.; Ruckert, M.; Schmitz, G.; Sierka, M.; Tapavicza, E.; Tew, D. P.; Van Wullen, C.; Voora, V. K.; Weigend, F.; Wodynski, A.; Yu, J. M. TURBOMOLE: Modular program suite for ab initio quantum-chemical and condensed-matter simulations. *J. Chem. Phys.* **2020**, *152*, 36.
(43) *TURBOMOLE V7.4.1, a development of University of Karlsruhe and Forschungszentrum Karlsruhe GmbH, 1989−2007, TURBOMOLE GmbH, since* 2007; available from http://www.turbomole.com.
(44) Douglas, M.; Kroll, N. M. Quantum Electrodynamical Corrections to the Fine Structure of Helium*. *Ann. Phys.* **1974**, *82*, 89−155.
(45) Hess, B. A. Relativistic electronic-structure calculations employing a two-component no-pair formalism with external-field projection operators. *Phys. Rev. A* **1986**, *33*, 3742−3748.
(46) Malmqvist, P.-Å.; Roos, B. O.; Schimmelpfennig, B. The restricted active space (RAS) state interaction approach with spin−orbit coupling. *Chem. Phys. Lett.* **2002**, *357*, 230−240.
(47) Roos, B. O.; Lindh, R.; Malmqvist, P. Å.; Veryazov, V.; Widmark, P. O. New relativistic ANO basis sets for actinide atoms. *Chem. Phys. Lett.* **2005**, *409*, 295−299.
(48) Roos, B. O.; Lindh, R.; Malmqvist, P.-Å.; Veryazov, V.; Widmark, P.-O. Main Group Atoms and Dimers Studied with a New Relativistic ANO Basis Set. *J. Phys. Chem. A* **2004**, *108*, 2851−2858.
(49) Feller, D. Application of systematic sequences of wave functions to the water dimer. *J. Chem. Phys.* **1992**, *96*, 6104−6114.
(50) Feller, D. The use of systematic sequences of wave functions for estimating the complete basis set, full configuration interaction limit in water. *J. Chem. Phys.* **1993**, *98*, 7059−7071.
(51) Karton, A.; Martin, J. M. L. Comment on: ″Estimating the Hartree-Fock limit from finite basis set calculations″ Jensen F (2005) Theor Chem Acc 113, 267. *Theor. Chem. Acc.* **2006**, *115*, 330−333.
(52) Aquilante, F.; Autschbach, J.; Baiardi, A.; Battaglia, S.; Borin, V. A.; Chibotaru, L. F.; Conti, I.; De Vico, L.; Delcey, M.; Galvan, I. F.; Ferre, N.; Freitag, L.; Garavelli, M.; Gong, X. J.; Knecht, S.; Larsson, E. D.; Lindh, R.; Lundberg, M.; Malmqvist, P. A.; Nenov, A.; Norell, J.; Odelius, M.; Olivucci, M.; Pedersen, T. B.; Pedraza-Gonzalez, L.; Phung, Q. M.; Pierloot, K.; Reiher, M.; Schapiro, I.; Segarra-Marti, J.; Segatta, F.; Seijo, L.; Sen, S.; Sergentu, D. C.; Stein, C. J.; Ungur, L.; Vacher, M.; Valentini, A.; Veryazov, V. Modern quantum chemistry with Open Molcas. *J. Chem. Phys.* **2020**, *152*, 25.
(53) Galván, I. F.; Vacher, M.; Alavi, A.; Angeli, C.; Aquilante, F.; Autschbach, J.; Bao, J. J.; Bokarev, S. I.; Bogdanov, N. A.; Carlson, R. K.; Chibotaru, L. F.; Creutzberg, J.; Dattani, N.; Delcey, M. G.; Dong, S. J. S.; Dreuw, A.; Freitag, L.; Frutos, L. M.; Gagliardi, L.; Gendron, F.; Giussani, A.; González, L.; Grell, G.; Guo, M. Y.; Hoyer, C. E.; Johansson, M.; Keller, S.; Knecht, S.; Kovacevic, G.; Källman, E.; Li Manni, G.; Lundberg, M.; Ma, Y. J.; Mai, S.; Malhado, J. P.; Malmqvist, P. A.; Marquetand, P.; Mewes, S. A.; Norell, J.; Olivucci, M.; Oppel, M.; Phung, Q. M.; Pierloot, K.; Plasser, F.; Reiher, M.; Sand, A. M.; Schapiro, I.; Sharma, P.; Stein, C. J.; Sorensen, L. K.; Truhlar, D. G.; Ugandi, M.; Ungur, L.; Valentini, A.; Vancoillie, S.; Veryazov, V.; Weser, O.; Wesolowski, T. A.; Widmark, P. O.; Wouters, S.; Zech, A.; Zobel, J. P.; Lindh, R. OpenMolcas: From Source Code to Insight. *J. Chem. Theory Comput.* **2019**, *15*, 5925−5964.
(54) Bryantsev, V. S.; Diallo, M. S.; Goddard, W. A., III Calculation of solvation free energies of charged solutes using mixed cluster/continuum models. *J. Phys. Chem. B* **2008**, *112*, 9709−9719.
(55) Kimura, T.; Choppin, G. R. Luminescence study on determination of the hydration number of Cm(III). *J. Alloys Compd.* **1994**, *213-214*, 313−317.
(56) Van Aert, R. C. M.; Jackson, D. A new justification of the Hartung-Knapp method for random-effects meta-analysis based on weighted least squares regression. *Res. Synth. Methods* **2019**, *10*, 515−527.
(57) Moog, H. C.; Voigt, W. *Thermodynamic Reference Database. Dielectric Constant, Vapor Pressure, and Density of Water and the Calculation of Debye-Hückel Parameters ADH, BDH, and Aϕ for Water. THEREDA Technical Paper*; 2011.

https://doi.org/10.1021/acs.inorgchem.1c01319
Inorg. Chem. 2021, 60, 10656−10673

(58) Huang, Q. R.; Kingham, J. R.; Kaltsoyannis, N. The strength of actinide-element bonds from the quantum theory of atoms-in-molecules. *Dalton Trans.* **2015**, *44*, 2554−2566.
(59) Kerridge, A. Quantification of f-element covalency through analysis of the electron density: insights from simulation. *Chem. Commun.* **2017**, *53*, 6685−6695.
(60) Lindqvist-Reis, P.; Réal, F.; Janicki, R.; Vallet, V. Unraveling the Ground State and Excited State Structures and Dynamics of Hydrated Ce^{3+} Ions by Experiment and Theory. *Inorg. Chem.* **2018**, *57*, 10111−10121.
(61) Ali, S. M. Role of Ligand Straining in Complexation of Eu^{3+}-Am^{3+} Ions by TPEN and PPDEN, Scalar Relativistic DFT Exploration in Conjunction with COSMO-RS. *ACS Omega* **2018**, *3*, 13104−13116.
(62) Lindqvist-Reis, P.; Klenze, R.; Schubert, G.; Fanghänel, T. Hydration of Cm^{3+} in Aqueous Solution from 20 to 200 °C. A Time-Resolved Laser Fluorescence Spectroscopy Study. *J. Phys. Chem. B* **2005**, *109*, 3077−3083.
(63) Banik, N. L.; Vallet, V.; Réal, F.; Belmecheri, R. M.; Schimmelpfennig, B.; Rothe, J.; Marsac, R.; Lindqvist-Reis, P.; Walther, C.; Denecke, M. A.; Marquardt, C. M. First structural characterization of Pa(IV) in aqueous solution and quantum chemical investigations of the tetravalent actinides up to Bk(IV): the evidence of a curium break. *Dalton Trans.* **2016**, *45*, 453−457.
(64) Qiao, Y.; Sergentu, D. C.; Yin, H.; Zabula, A. V.; Cheisson, T.; McSkimming, A.; Manor, B. C.; Carroll, P. J.; Anna, J. M.; Autschbach, J.; Schelter, E. J. Understanding and controlling the emission brightness and color of molecular cerium luminophores. *Abstr. Pap. Am. Chem. Soc.* **2018**, *140*, 4588−4595.
(65) Geissler, P. L. Temperature Dependence of Inhomogeneous Broadening: On the Meaning of Isosbestic Points. *J. Am. Chem. Soc.* **2005**, *127*, 14930−14935.

https://doi.org/10.1021/acs.inorgchem.1c01319
Inorg. Chem. 2021, 60, 10656−10673